Phosphorylation of Rab11-FIP2 regulates polarity in MDCK cells

Lynne A. Lapierre[a,b], Kenya M. Avant[a,b], Cathy M. Caldwell[a,b], Asli Oztan[c], Gerard Apodaca[c], Byron C. Knowles[a,b,d], Joseph T. Roland[a,b], Nicole A. Ducharme[d,e], and James R. Goldenring[a,b,d,f]

[a]Section of Surgical Sciences and Epithelial Biology Center, Vanderbilt University Medical Center, Nashville, TN 37232; [b]Nashville Veterans Affairs Medical Center, Nashville, TN 37212; [c]Department of Cell Biology and Physiology, University of Pittsburgh School of Medicine, Pittsburgh, PA 15261; [d]Department of Cell and Developmental Biology, Vanderbilt University School of Medicine, Nashville, TN 37232; [e]Center for Nuclear Receptor and Cell Signaling, University of Houston, Houston, TX 77204; [f]Vanderbilt-Ingram Cancer Center, Nashville, TN 37232

ABSTRACT **The Rab11 effector Rab11-family interacting protein 2 (Rab11-FIP2) regulates transcytosis through its interactions with Rab11a and myosin Vb. Previous studies implicated Rab11-FIP2 in the establishment of polarity in Madin–Darby canine kidney (MDCK) cells through phosphorylation of Ser-227 by MARK2. Here we examine the dynamic role of Rab11-FIP2 phosphorylation on MDCK cell polarity. Endogenous Rab11-FIP2 phosphorylated on Ser-227 coalesces on vesicular plaques during the reestablishment of polarity after either monolayer wounding or calcium switch. Whereas expression of the nonphosphorylatable Rab11-FIP2(S227A) elicits a loss in lumen formation in MDCK cell cysts grown in Matrigel, the putative pseudophosphorylated Rab11-FIP2(S227E) mutant induces the formation of cysts with multiple lumens. On permeable filters, Rab11-FIP2(S227E)–expressing cells exhibit alterations in the composition of both the adherens and tight junctions. At the adherens junction, p120 catenin and K-cadherin are retained, whereas the majority of the E-cadherin is lost. Although ZO-1 is retained at the tight junction, occludin is lost and the claudin composition is altered. Of interest, the effects of Rab11-FIP2 on cellular polarity did not involve myosin Vb or Rab11a. These results indicate that Ser-227 phosphorylation of Rab11-FIP2 regulates the composition of both adherens and tight junctions and is intimately involved in the regulation of polarity in epithelial cells.**

Monitoring Editor
Patrick Brennwald
University of North Carolina

Received: Aug 10, 2011
Revised: Apr 16, 2012
Accepted: Apr 24, 2012

INTRODUCTION

The establishment of polarity is a precisely regulated process in epithelial cells. Two junctional complexes—the tight and adherens junctions—separate the apical and basolateral domains of epithelial cells. The more apically positioned tight junction, consisting of ZO-1, occludin, claudin family members, and associated proteins, serves as a physical barrier between the two membrane domains and also regulates the paracellular permeability of the epithelial monolayer (Furuse, 2010; Steed *et al.*, 2010). The adherens junction facilitates cell–cell contact and is regulated partially by the cadherin and the catenin families of proteins (Harris and Tepass, 2010). Members of both junctions need to be trafficked to the correct domain for proper maintenance and function of the epithelial monolayer. One protein implicated in the trafficking of E-cadherin to the adherens junction is the small GTPase Rab11a (Desclozeaux *et al.*, 2008). Recent investigations indicated that both Rab11a and Rab8a, through their interactions with myosin Vb, influence the initiation of lumen formation in Madin–Darby canine kidney (MDCK) cells (Roland *et al.*, 2011).

Rab11a and its effectors, the Rab11-family interacting proteins (Rab11-FIPs), are well-documented participants in the regulation of apical membrane recycling and transcytosis in epithelial cells (for review see Jing and Prekeris, 2009). Rab11-family interacting

This article was published online ahead of print in MBoC in Press (http://www.molbiolcell.org/cgi/doi/10.1091/mbc.E11-08-0681) on May 2, 2012.

Address correspondence to: James R. Goldenring (jim.goldenring@vanderbilt.edu).

Abbreviations used: PBS, phosphate-buffered saline; PCX, gp135/podocalyxin; phospho-S227-Rab11-FIP2, Rab11-FIP2 phosphorylated on Ser-227; Rab11-FIP2, Rab11-family interacting protein 2; RT, room temperature; TBS, Tris-buffered saline.

protein 2 (Rab11-FIP2) forms a ternary complex with Rab11 and the motor protein myosin Vb to regulate basolateral-to-apical transcytosis in MDCK cells (Hales *et al.*, 2002; Ducharme *et al.*, 2007). The Rab11-FIP2/Rab11a/myosin Vb complex participates in the trafficking of a variety of cargoes in different cells. In nonpolar cells, transferrin receptor recycling (Hales *et al.*, 2002; Lindsay and McCaffrey, 2002), recycling of epidermal growth factor receptors (Cullis *et al.*, 2002), cholesterol-regulated translocation of NPC1L1 (Chu *et al.*, 2009), and GLUT4 and FAT/CD36 translocation (Schwenk *et al.*, 2007) are all influenced by Rab11a. In polarized epithelial cells, transcytosis of the polymeric immunoglobulin A (IgA) receptor (Lapierre *et al.*, 2001; Ducharme *et al.*, 2007), apical recycling of aquaporin-2 (Nedvetsky *et al.*, 2007), and apical trafficking and budding of respiratory syncytial virus (Brock *et al.*, 2003; Utley *et al.*, 2008) are all regulated by Rab11a and Rab11-FIP2. Rab11-FIP2 also associates with Eps15 homology domain 3, and this association is important in trafficking from the cell periphery to the endocytic recycling compartment in HeLa cells (Naslavsky *et al.*, 2006).

Previous investigations demonstrated that Par1b/MARK2 regulates the adoption of proper polarized membrane domains by MDCK cells (Cohen *et al.*, 2004, 2011). In addition, Rab11-FIP2 is a substrate for MARK2/EMK1/Par-1b, and its phosphorylation is necessary for the timely reestablishment of polarity in MDCK cells (Ducharme *et al.*, 2006). Here we sought to examine in greater detail the influence of this critical phosphorylation event on the establishment of polarity in MDCK cells. Phosphorylation of endogenous Rab11-FIP2 on Ser-227 occurred coincident with the establishment of polarity and subsequently decreased after epithelial polarization. MDCK cells overexpressing Rab11-FIP2(S227A), which cannot be phosphorylated by MARK2, formed cysts in three-dimensional cultures, but these cysts did not complete maturation and hollow out the central lumen. In contrast, expression of a phosphomimetic Rab11-FIP2(S227E) analogue caused the formation of multiple lumens within cysts and also altered the composition of both the tight and adherens junctions. Unlike the trafficking of polymeric IgA and other cargoes previously associated with Rab11-FIP2, the effects of phospho-S227-Rab11-FIP2 on establishment of polarity were independent of myosin Vb and Rab11a. These findings indicate that phosphorylation of Rab11-FIP2 by MARK2 is a critical regulator of the establishment of polarity in MDCK cells.

RESULTS

Endogenous Rab11-FIP2 is phosphorylated on Ser-227 at sites of polarity establishment

Rab11-FIP2 is phosphorylated on Ser-227 by Par1b/EMK1/MARK2, a serine kinase involved in cellular polarity (Cohen *et al.*, 2004; Ducharme *et al.*, 2006). Our previous investigations indicated that expression of a Rab11-FIP2 mutant that could not be phosphorylated by MARK2, Rab11-FIP2(S227A), led to deficits in the reestablishment of polarity in MDCK cells after calcium switch (Ducharme *et al.*, 2006). We produced a rabbit polyclonal antibody against phosphorylated Ser-227 in Rab11-FIP2 (for validation see Supplemental Figure S1). We predicted that Rab11-FIP2 would be phosphorylated on Ser-227 during the establishment of polarity. To determine if and when endogenous Rab11-FIP2 is phosphorylated on Ser-227 during cell polarization, we examined two models for the establishment of polarity: recovery from monolayer wounding and recovery from calcium switch. In the wounding paradigm, MDCK cells were grown for 5 d postconfluence on Transwell filters. A scratch wound was then made through the center of the monolayer, and the cells were allowed to recover for 48 h. Rab11-FIP2 phosphorylated at Ser-227 (phospho-S227-Rab11-FIP2) was observed within cells on the leading edge of the wound (Figure 1A), both on large vesicular structures and as a tight line costaining with p120-catenin on the leading edge of cells. At higher optical zoom on another area of the wound (Figure 1B) the phospho-S227-Rab11-FIP2 was accumulated at the corners of the cell's leading edge along with p120 (arrow, Figure 1B). This finding is in line with previous observations in which the junctional proteins p120 and E-cadherin moved in from the corners of cells during the reestablishment of cell–cell junctions (Nejsum and Nelson, 2007).

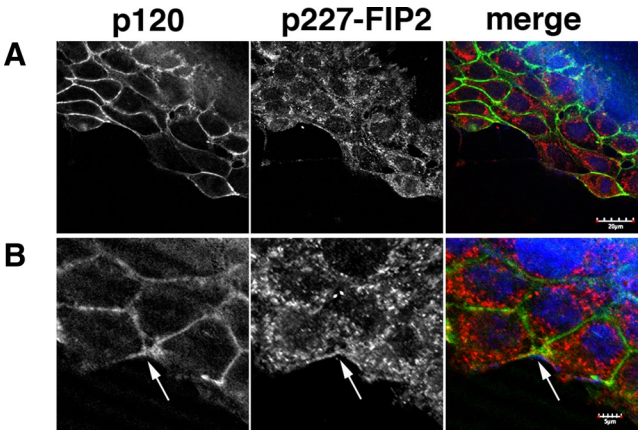

FIGURE 1: Endogenous Rab11-FIP2 is phosphorylated on Ser-227 during wound healing. MDCK cells were grown 5 d postconfluence on Transwell filters. The monolayer was wounded and allowed to recover for 48 h before fixing. The cells were stained for p120 (green in merge), Ser-227–phosphorylated Rab11-FIP2 (red in merge), and DAPI (blue in merge). (A, B) Different areas of the monolayer at different optical zooms. Arrow in B indicates a p120 plaque with phospho-S227-Rab11-FIP2. Bar, 20 μm (A), 5 μm (B).

To examine whether MARK2 is the kinase responsible for phosphorylating Rab11-FIP2 on Ser-227 during the establishment of polarity, we investigated the level of phosphorylation of Ser-227 in Rab11-FIP2 by using an MDCK cell line with inducible expression of MARK2 shRNA, MARK2-KD (Elbert *et al.*, 2006). In subconfluent conditions, endogenous phospho-S227-Rab11-FIP2 was observed along the edges of the cell islands, especially accumulating at the corners of cells with p120 (Figure 2, MARK2-KD-off). In the MDCK cell line in which MARK2 expression is knocked down (Figure 2, MARK2-KD-on), there was a 50% reduction in the mean intensity of the phospho-S227-Rab11-FIP2 staining. This result correlates well with the 50% knockdown of MARK2 expression achieved in this cell line (Elbert *et al.*, 2006). Similar results were observed when the MARK2-KD cell line was used in the wounding and calcium switch models of polarity (unpublished data). Of interest, in the subconfluent cells, there was also a 50% decrease in p120 staining intensity in the MARK2-KD cells (Figure 2). This reduction of p120 may be caused not only by the reduced phosphorylation of Rab11-FIP2, but also by decreased phosphorylation of other MARK2 substrates (Matenia and Mandelkow, 2009).

Previous work from our lab demonstrated that mutating the Ser-227 to an alanine still allowed Rab11-FIP2 to interact with Rab11a, and myosin Vb and did not alter apical recycling or transcytosis but did interfere with the ability of cells to polarize after calcium switch (Ducharme *et al.*, 2006). We produced a putative phosphomimetic GFP-Rab11-FIP2(S227E)–expressing tet-off cell line in MDCK cells similar to the tet-off GFP-Rab11-FIP2(S227A)–expressing cell line used in our previous work (Ducharme *et al.*, 2006). As with GFP-Rab11-FIP2(S227A) (Ducharme *et al.*, 2006),

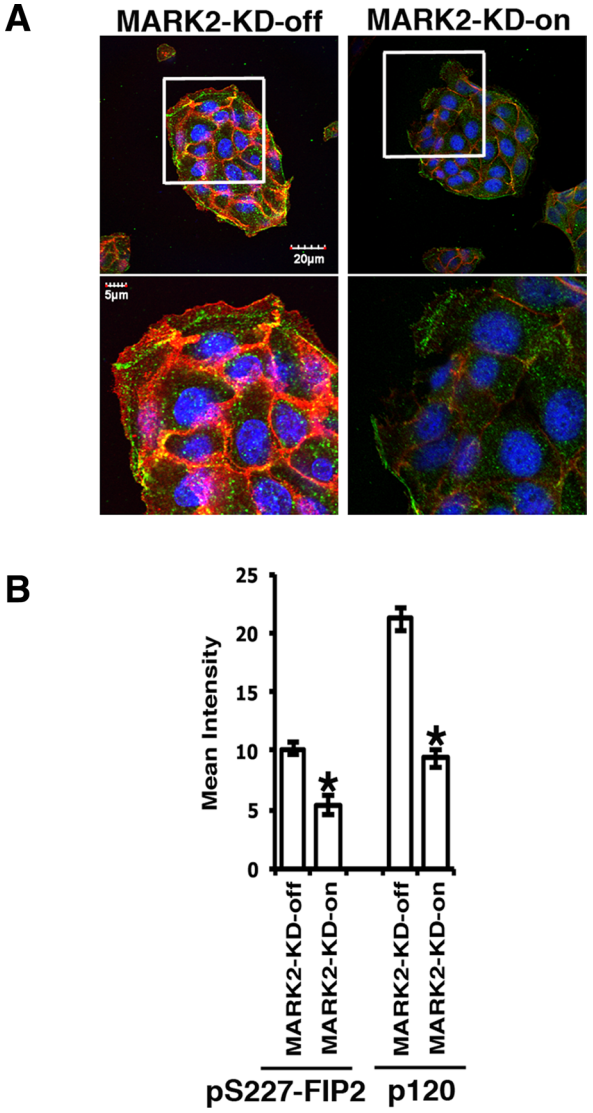

FIGURE 2: Knockdown of MARK2 reduces phosphorylation of Rab11-FIP2 on Ser-227. MDCK cell lines either with knockdown of MARK2 (MARK2-KD-on) or without knockdown (MARK2-KD-off) were plated at subconfluence onto coverslips, fixed, and stained for phospho-S227-Rab11-FIP2 (green in A), p120 (red in A), and DAPI (blue in A). (A) Representative images; bottom, zooms of the boxed areas above. Bar, 20 μm (top), 5 μm (bottom). (B) Quantitation of mean fluorescence calculated using Image J. Twelve fields each from three separate experiments were used for the calculations. *$p < 0.0001$.

GFP-Rab11-FIP2(S227E) was able to interact with Rab11a and myosin Vb and did not interfere with apical recycling or basolateral to apical transcytosis of polymeric IgA (Figure 3, A–C). Whereas the overexpressed GFP-Rab11-FIP2(S227E) chimera was pulled into the Cherry-myosin Vb tail-containing compartment, the endogenous phospho-S227-Rab11-FIP2 did not colocalize with myosin Vb tail (Figure 3D). This difference in localization with the myosin Vb tail construct may be due to the overexpression of the GFP-Rab11-FIP2(S227E) construct versus the endogenous pool of phospho-S227-Rab11-FIP2. With costaining of nonpolar MDCK cells with antibodies against myosin Vb and phospho-S227-Rab11-FIP2, we also observed no colocalization between the two proteins (Figure 3E).

To examine the distribution of Rab11-FIP2 phosphorylated at Ser-227 in MDCK cells during the reestablishment of polarity, we used the calcium switch model of cell polarization (Gerardo *et al.*, 1991). All of the GFP-Rab11-FIP2 cell lines were maintained in doxycycline until the time of plating onto Transwell filters. The Transwell filters were plated at confluence without doxycycline, allowing the cells to contact and establish polarity soon after plating and before the expression of the GFP-Rab11-FIP2 constructs. To examine the distribution of phospho-S227-Rab11-FIP2 in MDCK cells without chimera expression, the GFP-Rab11-FIP2(S227E) cell line was grown for 5 d postconfluence on Transwell filters in the presence of doxycycline to inhibit chimera expression (designated as "off"). Similar results were obtained when the parental MDCK cell line was calcium switched and stained (unpublished data). In MDCK cells without calcium switch, antibodies against phospho-S227-Rab11-FIP2 stained only a few large vesicular structures that tended to be in the corners of cells (Figures 4A and 5A). If the images of the nonswitched cells were brightened above the levels used for the other time points, a dispersed vesicular pattern of phospho-S227-Rab11-FIP2 could also be seen. After treating these cells for 18–24 h in low-calcium media, we observed some dispersed phospho-S227-Rab11-FIP2 immunoreactivity. Thirty minutes after refeeding the cells with calcium-containing media, we observed phospho-S227-Rab11-FIP2 immunoreactivity in the apical one-third of the cells in vesicles and along the lateral edge, especially in newly formed corners of cells in the repolarizing monolayer (Figures 4A and 5A). At 60 and 90 min of recovery, phospho-S227-Rab11-FIP2 was still seen in the apical one-third of the cells but was also observed at the basal surface of the cells out near the periphery (Figures 4A and 5A). Similar results were observed in parental nontransfected MDCK cells (unpublished data). These results indicate that there is a small, cytoplasmic population of phospho-S227-Rab11-FIP2 in MDCK cells before calcium switch that increased and aggregated during calcium switch recovery.

To investigate whether the pool of Rab11-FIP2 phosphorylated on Ser-227 required myosin Vb for trafficking, we performed a calcium switch assay using an MDCK cell line stably expressing a short hairpin RNA (shRNA) targeting canine myosin Vb (Roland *et al.*, 2011). Figure 3F depicts this cell line, in which, 30 min into calcium switch recovery, the phospho-S227-Rab11-FIP2 converged near the basolateral membranes (Figure 3F), similar to the pattern seen in nonexpressing cells (Figures 4A and 5A, GFP-FIP2(S227E)-off). Thus trafficking of phospho-S227-Rab11-FIP2–containing vesicles does not require myosin Vb.

In GFP-Rab11-FIP2-wild type–expressing cells, we observed a pattern similar to that for endogenous Rab11-FIP2 phosphorylation. Immunostaining for phospho-S227-Rab11-FIP2 localized in apically distributed vesicles in the nonswitched cells and to some extent in the cells grown in the low-calcium media. As the cells recovered from the calcium switch, the phospho-S227-Rab11-FIP2 staining redistributed to a more collapsed pattern in both apical and basal regions of the cells (Figures 4B and 5B). Of interest, in the doxycycline-treated GFP-Rab11-FIP2(S227E)-off cells (Figures 4A and 5A), the endogenous phospho-S227-Rab11-FIP2 was observed at the periphery of the cells near cell–cell contacts. In contrast, wild-type GFP-Rab11-FIP2 phosphorylated on Ser-227 was not localized to the periphery but instead was observed in the coalesced GFP-Rab11-FIP2–containing vesicular structure, indicating a mislocalization of Ser-227–phosphorylated GFP-Rab11-FIP2 to a more central structure. The endogenous phosphoS227-Rab11-FIP2 could still be faintly seen at the lateral edges of the cells. Thus, whereas the overexpressed GFP-Rab11-FIP2WT chimera can be phosphorylated on Ser-227 during polarization, it was mislocalized to a central

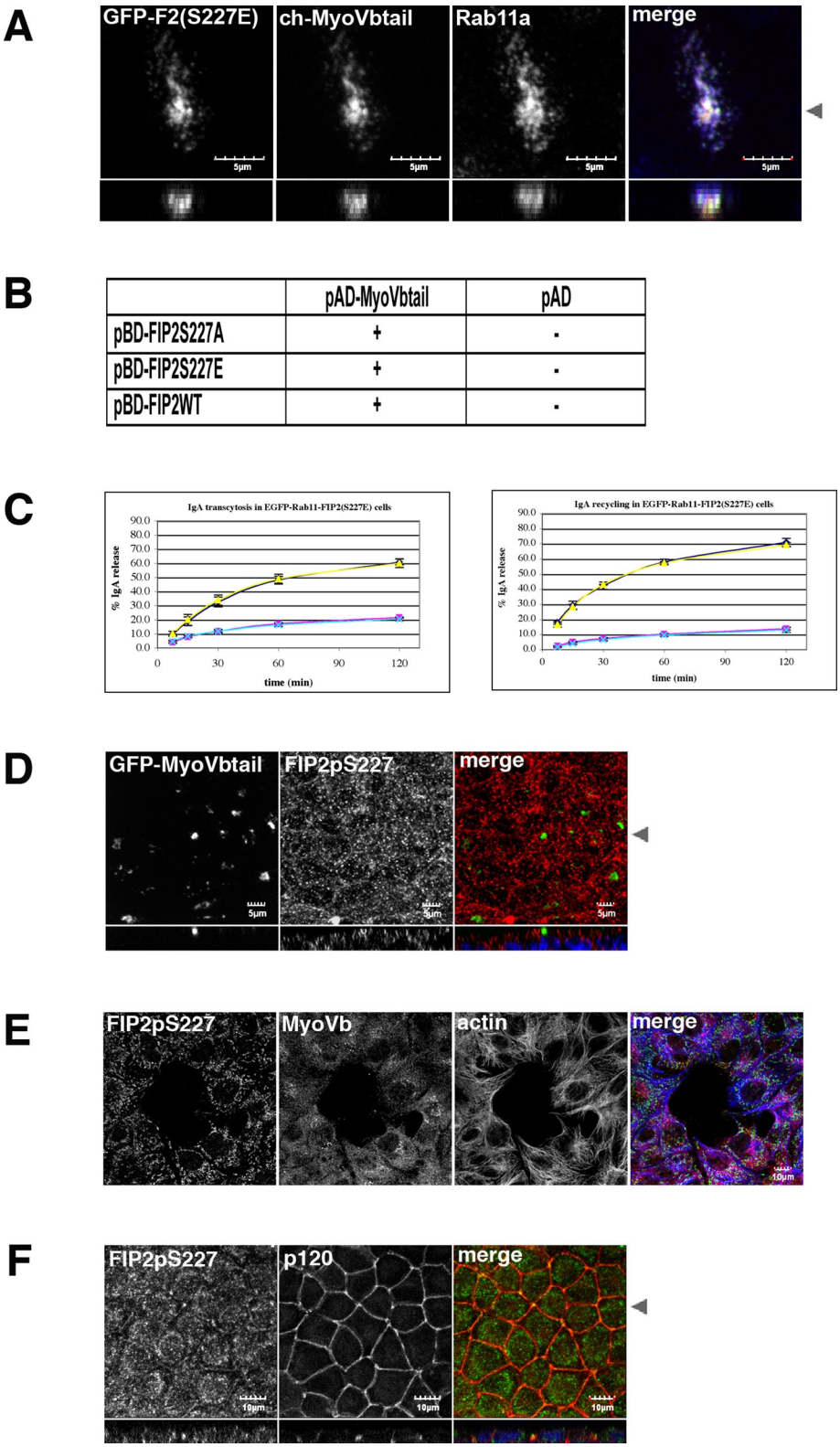

FIGURE 3: Although GFP-Rab11-FIP2(S227E) still interacts with myosin Vb tail and does not affect IgA transcytosis or apical recycling, endogenous phosphor-S227-Rab11-FIP2 does not. (A) The GFP-Rab11-FIP2(S22E) (green in merge) cell line was transiently transfected with Cherry-myosin Vb tail (red in merge) and grown without doxycycline for 5 d postconfluence on Transwell filters. The cells were fixed and stained for Rab11a (blue in merge). Both GFP-Rab11-FIP2(S227E) and Rab11a were pulled into the Cherry-myosin Vb tail compartment. Bar, 5 μm. (B) Rab11-FIP2WT and the Ser-227 mutants were tested against a myosin Vb tail construct and empty vector in a yeast two-hybrid assay. All three of the Rab11-FIP2 constructs interacted with the myosin Vb tail but not the empty vector. (C) The GFP-Rab11-FIP2(S227E) cell line was grown for 5 d postconfluence on Transwell filters in the presence ("off"; dark blue and pink lines) or absence ("on"; yellow and light blue lines) of doxycycline. Left, the transcytosis assay; right, the apical recycling assay. Dark blue and yellow lines indicate that media were collected from the apical side of the Transwell filter, and pink and light blue indicate that media were collected from the basal side of the Transwell filter. (D) The GFP-myosin Vb tail line was grown for 5 d postconfluence on Transwell filters, fixed, and stained for phospho-S227-Rab11-FIP2. The pS227-FIP2 stained as small punctate structures throughout the cell and did not collapse into the GFP-myosin Vb tail structure. Bar, 5 μm. (E) MDCK cells were grown on coverslips, fixed, and stained for phospho-S227-Rab11-FIP2 (green in merge), myosin Vb (red in merge), and actin (blue in merge). Bar, 10 μm. (F) An MDCK cell line stably expressing an shRNA targeted to canine myosin Vb was incubated overnight with Ca-free media and then switched back to calcium-containing media for 30 min, fixed, and stained for phospho-S227-Rab11-FIP2 and p120. The p227-FIP2 converged on the lateral membrane similar to what was seen in control cells (Figures 4A and 5A). Bar, 10 μm.

structure. This indicates that the pool of Rab11-FIP2 that is involved in polarity is limited, potentially through limited amounts of binding partners within the polarizing cell.

When GFP-Rab11-FIP2(S227E) expression was induced in the absence of doxycycline, GFP-Rab11-FIP2(S227E) localized in a tubular pattern within the apical portion of the cell. During the low-calcium incubation, the GFP-Rab11-FIP2(S227E) clustered in the apical portion of the cell. Then, as the cells recovered from the calcium switch, this GFP-Rab11-FIP2(S227E) coalesced and moved deeper in the cell, so that by 90 min of recovery, most of the GFP-Rab11-FIP2(S227E) was found in the basal portion of the cell (Figures 4C and 5C). Little endogenous phospho-S227-Rab11-FIP2 staining was seen in cells expressing GFP-Rab11-FIP2(S227E) at any time point. The anti–phospho-S227-Rab11-FIP2 antibody did not recognize the GFP-Rab11-FIP2(S227E) phosphomimetic mutation.

Endogenous phospho-S227-Rab11-FIP2 and GFP-Rab11a do not colocalize

To investigate whether Rab11a was involved with phospho-S227-Rab11-FIP2 during repolarization of the cells, we examined an MDCK cell line stably expressing GFP-Rab11a during calcium switch. Unfortunately, our antibody that recognizes canine Rab11a and the anti–phosphoS227-Rab11-FIP2 are

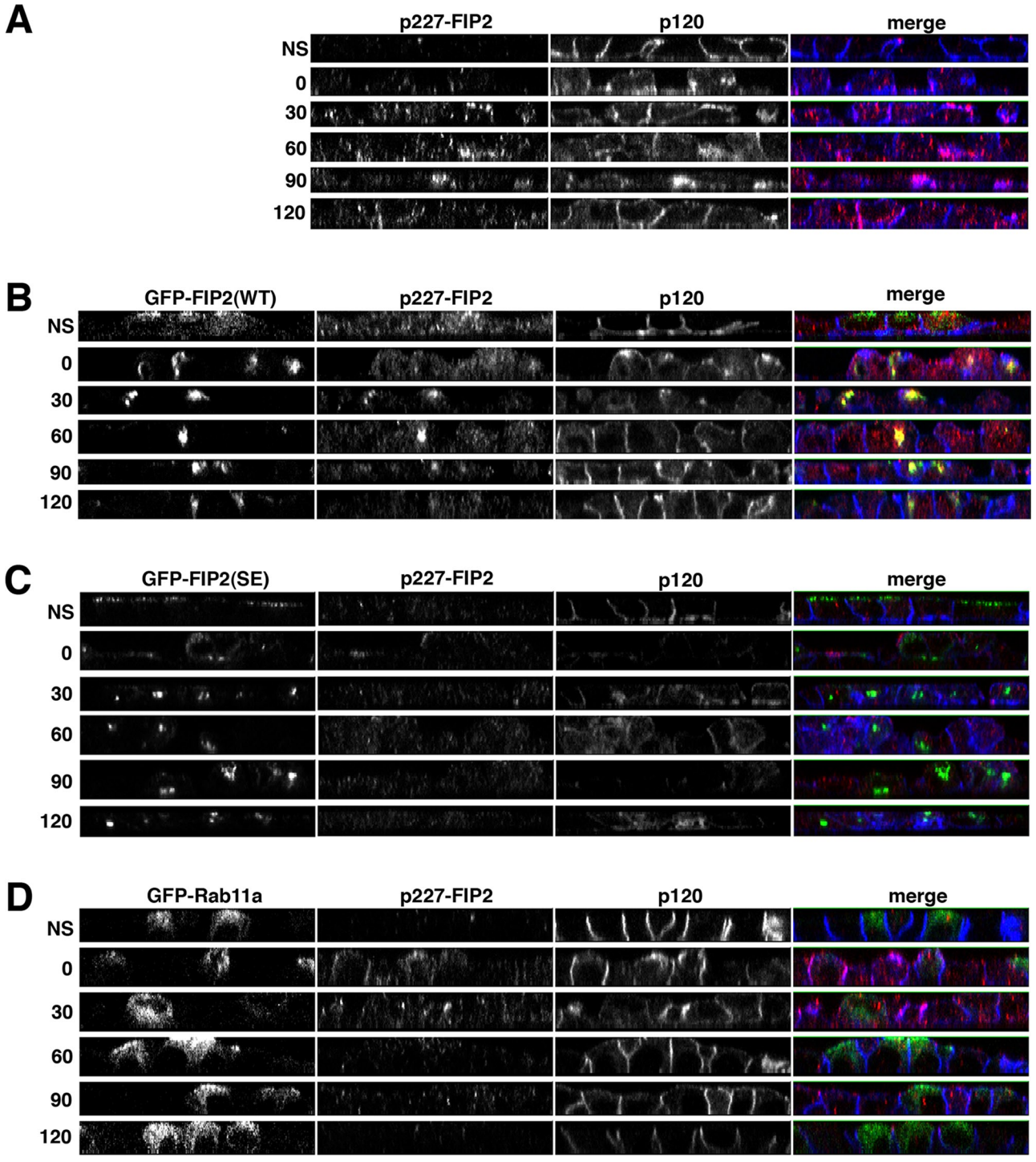

FIGURE 4: Endogenous Rab11-FIP2 is phosphorylated on Ser-227 during recovery from calcium switch. The GFP-Rab11-FIP2 and GFP-Rab11a cell lines (green in merge) were grown for 5 d postconfluence on Transwells in doxycycline-free media ("on"; B, C) or doxycycline-containing media ("off"; A), fixed, and stained for Ser-227–phosphorylated Rab11-FIP2 (red in merge) and p120 (blue in merge). The cell lines examined were (A) GFP-Rab11-FIP2(S227E)-off, (B) GFP-Rab11-FIP2-WT-on, (C) GFP-Rab11-FIP2(S227E)-on, and (D) GFP-Rab11a. The numbers on the left represent minutes of recovery after the cells were refed with calcium-containing media. NS, nonswitched.

both rabbit polyclonal antibodies. Therefore we could not costain for both endogenous proteins. Unlike wild-type GFP-Rab11-FIP2 and GFP-Rab11-FIP2(S227E), the majority of the GFP-Rab11a remained in a subapical vesicular distribution during the calcium switch (Figures 4D and 5D). We did not observe any GFP-Rab11a at the periphery with the endogenous phospho-S227-Rab11-FIP2. Of interest, we did observe staining for phospho-S227-Rab11-FIP2 in the cell periphery earlier in the calcium recovery in cells expressing green fluorescent protein (GFP)-Rab11a, with the highest levels of phospho-S227-Rab11-FIP2 immunostaining at 0 and 30 min of recovery. These results suggest that Rab11-FIP2's function in cell polarity is Rab11a independent.

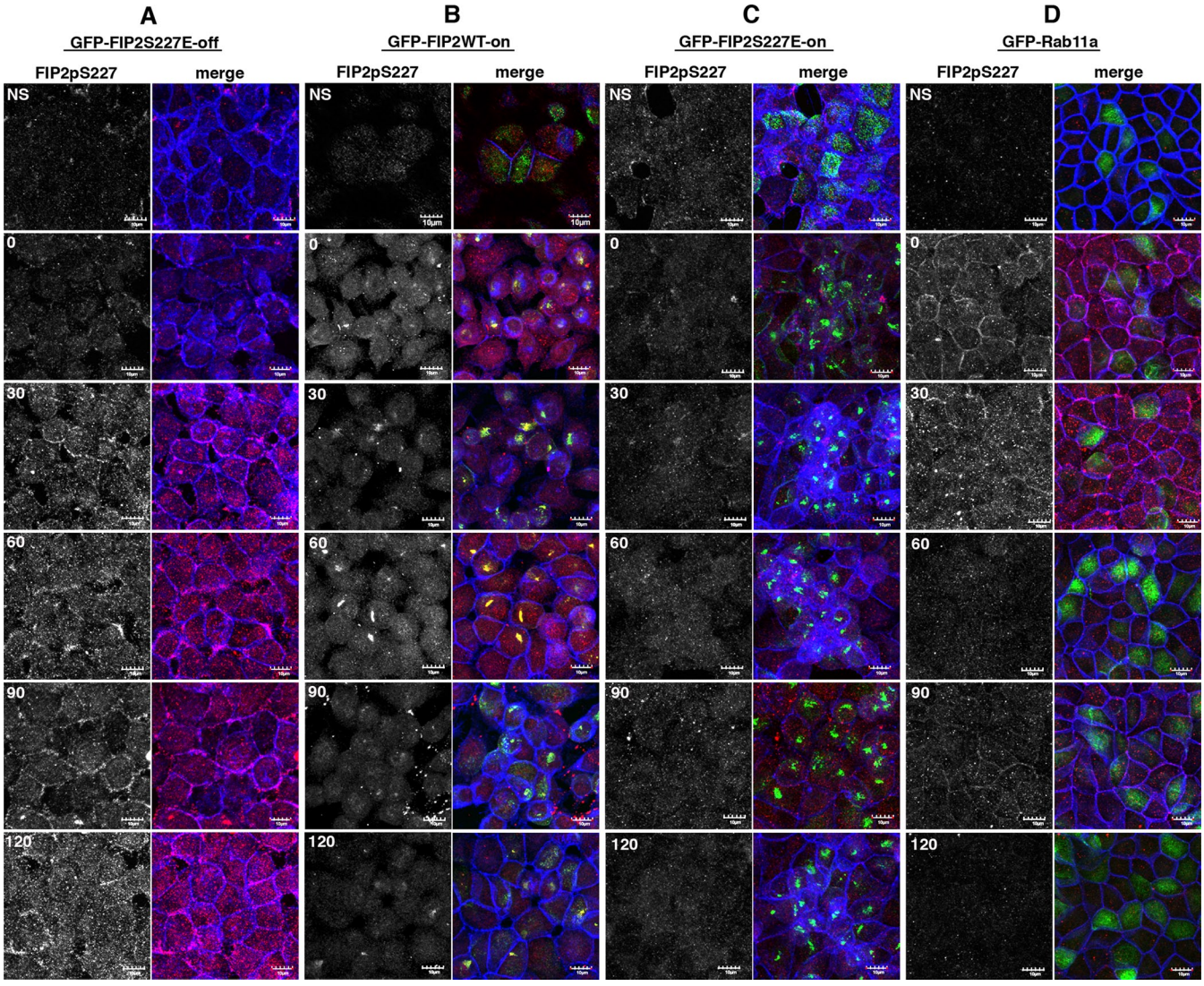

FIGURE 5: The corresponding *xy* images of Figure 3. Endogenous Rab11-FIP2 is phosphorylated on Ser-227 during recovery from calcium switch. The GFP-Rab11-FIP2 cell lines (green in merge) were grown for 5 d postconfluence on Transwell filters, fixed, and costained for Ser-227–phosphorylated Rab11-FIP2 (first column and red in merge) and p120 (blue in merge). The cell lines are (A) GFP-Rab11-FIP2(S227E)-off, (B) GFP-Rab11-FIP2-WT-on, (C) GFP-Rab11-FIP2(S227E)-on, and (D) GFP-Rab11a. Bar, 10 μm. The numbers on the left represent minutes of recovery after the cells were refed with calcium-containing media. NS, nonswitched.

Overexpression of Rab11-FIP2 Ser-227 mutants induces atypical cyst formation in Matrigel

When GFP-Rab11-FIP2(S227E)–expressing cells were grown on permeable supports (Transwell filters), the monolayer did not exhibit any gross morphological changes. However, when grown in a more stringently polar manner, as seen in cysts within a Matrigel matrix, drastic morphological changes were observed. The GFP-Rab11-FIP2(S227E)–off cells (Figure 6A and Supplemental Video S1) formed typical hollow cysts, similar to the pattern others have published for MDCK cells (Martin-Belmonte and Mostov, 2008; Martin-Belmonte *et al.*, 2008) and replicated in our studies with parental MDCK cells (unpublished data). These smooth, round cysts consisted of a single layer of cells forming a hollow lumen with the apical side of the cells facing into the lumen, as indicated by apical gp135/podocalyxin (PCX) staining in Figure 6A and Supplemental Video S1. Cells expressing wild-type GFP-Rab11-FIP2 formed round, hollow cysts, but these often retained some condensed nuclei within the lumen (Figure 6B). In contrast, cells expressing GFP-Rab11-FIP2(S227A) formed round cysts, but, unlike the nonexpressing cells, there were still cells, some with condensed nuclei, within the luminal area (Figure 6C). The outer layer of cells did form a single layer with an internally facing apical membrane, but the lumen failed to complete maturation and hollow out. The most dramatic morphological change was observed with the cells expressing GFP-Rab11-FIP2(S227E) (Figure 6, D and E, and Supplemental Videos S2 and S3). This cell line formed cysts that appeared to have multiple lumens similar to but not exactly like the pattern seen when MARK2 is overexpressed (Cohen *et al.*, 2004). On closer examination of three-dimensional images (Supplemental Videos S2 and S3), lateral lumens can be observed in the periphery of the cysts, but multiple-cyst lumina are also contained within the lumen of the large cyst. These studies suggested that expression of the pseudophosphorylated Rab11-FIP2(S227E) promoted unregulated apical lumen formation. In the mature

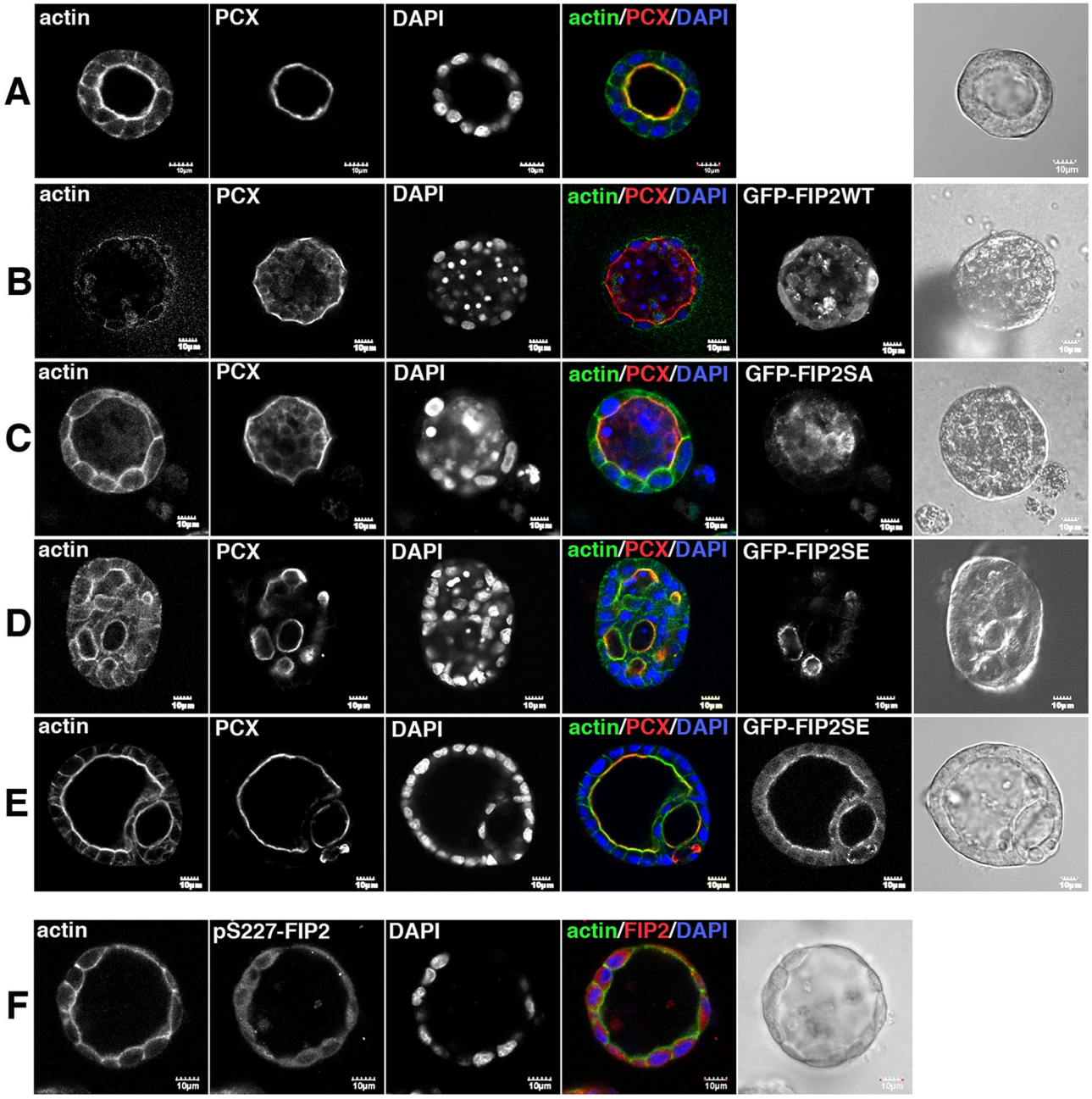

FIGURE 6: Overexpression of GFP-Rab11-FIP2 wild type and mutants alters the morphology of cysts. (A) GFP11-FIP2(S227E) cells were grown for 14 d in Matrigel with doxycycline ("off") and were stained for actin (green in merge), podocalyxin/gp135 (red in merge), DAPI (blue in merge). GFP-Rab11-FIP2-WT (B), GFP-Rab11-FIP2(S227A) (C), and GFP-Rab11-FIP2(S227E) (D, E) cell lines were grown without doxycycline (on) for 14 d and stained as in A. In the GFP-Rab11-FIP2-WT cell line, 90% of the cysts exhibited a single-lumen morphology as shown here. However, for GFP-Rab11-FIP2(S227A)–expressing cells 84% of cysts had a filled-lumen morphology. In Rab11-FIP2(S227E)–expressing cells, 87% of cysts showed multiple lumens. (F) MDCK cells were grown for 14 d in Matrigel and then stained for phospho-S227-Rab11-FIP2 (green in merge), podocalyxin/gp135 (red in merge), and DAPI (blue in merge). Corresponding videos are available for the GFP-Rab11-FIP2(S227E) "off" (Supplemental Video S1) and GFP-Rab11-FIP2(S227E) "on" (Supplemental Videos S2 and S3) cell lines and for the phospho-S227-Rab1-FIP2–stained cyst (Supplemental Video S4). Bar, 10 μm.

cysts, endogenous phospho-S227-Rab11-FIP2 staining was observed as faint puncta throughout the cell, with concentrations of brighter staining below the apical surface (Figure 6F and Supplemental Video S4).

We investigated the expression of phospho-S227-Rab11-FIP2 in cells at the start of cyst formation when the apical membrane is first being established, as indicated by PCX localization (Bryant *et al.*, 2010). At the two-cell stage, when PCX localizes to the adjoining membrane between the two cells, we observed phospho-S227-Rab11-FIP2 throughout the cell with an increased density below the adjoining membrane, but no colocalization with PCX was observed (Figure 7A and Supplemental Video S5). At the three-cell stage, the

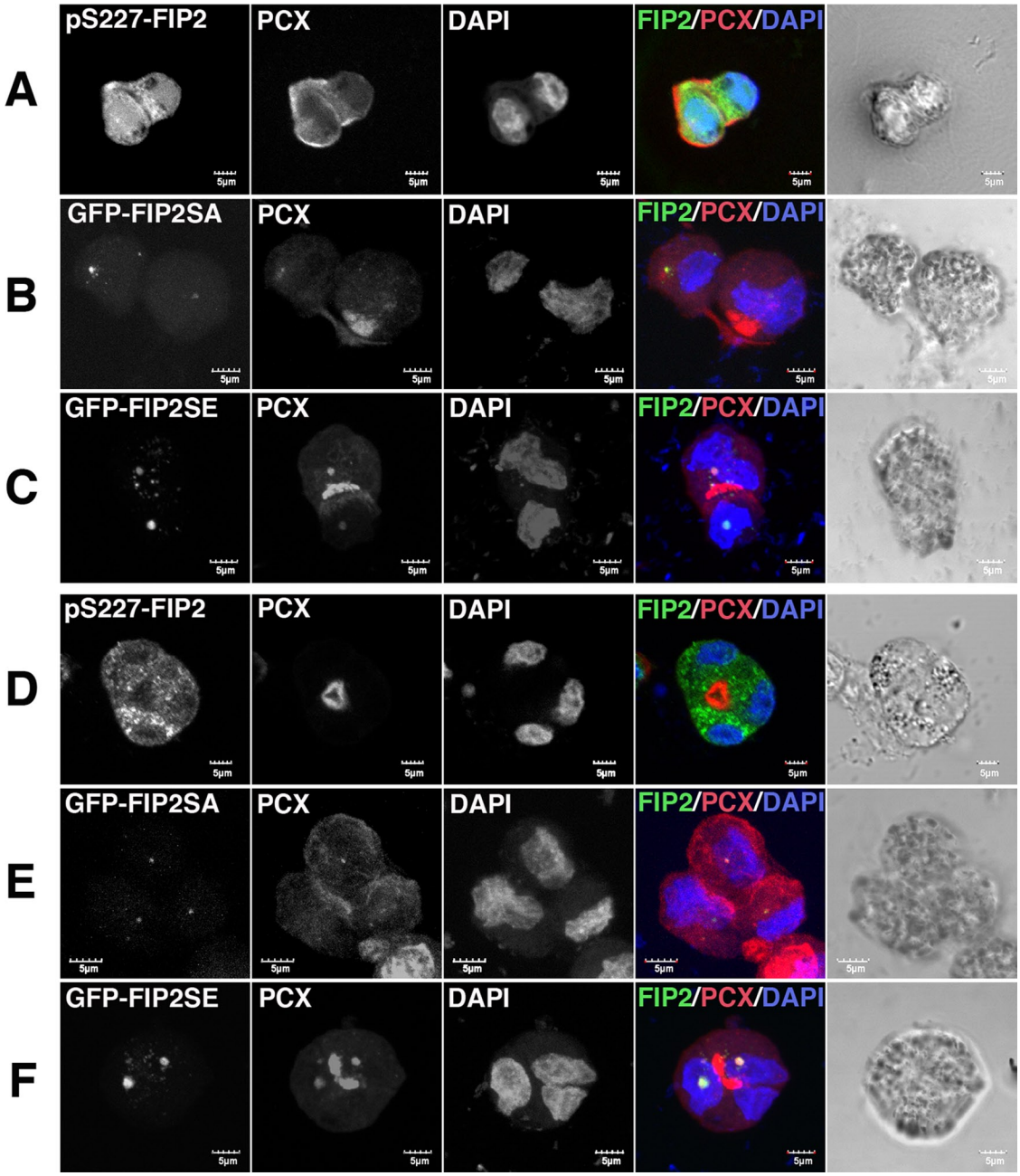

FIGURE 7: Overexpression of GFP-Rab11-FIP2 wild type and mutants alters the early morphology of cysts. MDCK, GFP-Rab11-FIP2(S227A), and GFP11-FIP2(S227E) cells were grown for 24–48 h in Matrigel without doxycycline ("on"). MDCK cells were stained for phospho-S227-Rab11-FIP2 (green in merge), and all three cell lines were stained for podocalyxin/gp135 (red in merge) and DAPI (blue in merge). (A–C) Two-cell stage. (D–F) Three-cell stage. In the GFP-Rab11-FIP2(S227A) cell line, 75% of the two-cell-stage cysts and 81% of the three-cell-stage cysts exhibited a morphology as shown here, whereas for GFP-Rab11-FIP2(S227E), 79% of the two-cell-stage cysts and 78% of the three-cell-stage cysts showed morphologies as depicted. Corresponding videos are available for the MDCK (Supplemental Videos S5 and S6), GFP-Rab11-FIP2(S227A) (Supplemental Videos S7 and S8), and GFP-Rab11-FIP2(S227E) (Supplemental Videos S9 and S10) cell lines. Bar, 5 µm.

lumen consisted of a central spot equally shared by all the cells. Again the phospho-S227-Rab11-FIP2 was present throughout the cell and below the forming apical lumen (Figure 7D and Supplemental Video S6). In the GFP-Rab11-FIP2(S227A)–overexpressing cell line, PCX localization to the site of lumen formation was delayed until the three-cell stage, with some PCX still localized to vesicles within the cells (Figure 7, B and E, and Supplemental Videos S7 and S8). In the GFP-Rab11-FIP2(S227E) cell line, PCX did aggregate at the adjacent membranes, but at the three-cell stage the lumen showed an elongated, dumbbell shape that extended between pairs of cells, as opposed to the round, central, shared lumen normally observed (Figure 7, C and F, and Supplemental Videos S9 and S10). In the mature lumen, both GFP-Rabll-FIP2 mutants were located to vesicles below the apical membrane. In the early cysts,

both mutants were in a more centrally collapsed structure that contained some PCX.

The S227E pseudophosphorylation mutant of Rab11-FIP2 alters the composition of cellular junctions

Given that the composition of cellular junction can influence polarity and the kinase MARK2 is involved in polarity (Cohen *et al.*, 2004), we investigated whether the composition of the cellular junctions in the GFP-Rab11-FIP2(S227E) cell line was altered. Whereas E-cadherin remained at the adherens junction in wild-type GFP-Rab11-FIP2– and GFP-Rab11-FIP2(S227A)–expressing cells, in the GFP-Rab11-FIP2(S227E)–expressing cells, E-cadherin was lost from the junctions (Figure 8A). Indeed this prominent loss of E-cadherin protein was also seen by Western blot analysis (Figure 8B). No statistically significant alteration in E-cadherin mRNA expression was observed (Figure 8C). Treating the cells with lysosome or proteasome inhibitors had no effect on the levels of E-cadherin in the GFP-Rab11-FIP2(S227E) cell line (unpublished data). Of interest, K-cadherin (Figure 8, A and B) protein expression was increased when the GFP-Rab11-FIP2 chimeras were expressed, whereas the GFP-Rab11-FIP2WT and GFP-Rab11-FIP2(S227E) cell lines had less mRNA expression. These results were also observed when the cells were grown as cysts in Matrigel (unpublished data).

We next examined the effects of Rab11-FIP2(S227E) expression on tight junction components. ZO-1 was not altered in any of the cells lines, but occludin was lost from the cells overexpressing GFP-Rab11-FIP2(S227E) (Figure 9, A and B). No differences were observed in MDCK cells expressing either wild-type GFP-Rab11-FIP2 (Figure 9, A and B) or the GFP-Rab11-FIP2(S227A) (unpublished data). Similar to E-cadherin, no difference in occludin mRNA expression was observed (Figure 9C). Of interest, we did not observe a significant change in the transepithelial resistance (TER; Figure 9D) in any of the cell lines. Therefore we investigated whether there were any changes in the expression of the claudins. Claudin 1 protein and mRNA levels and protein localization were not changed among the cell lines (Figure 10, A, D, and E). In the cells without chimera expression (doxycycline-treated GFP-Rab11-FIP2(S22E)–off cells) the majority of claudin 2 was observed in vesicles near the periphery of the cell. However, in the GFP-Rab11-FIP2(S227E)– and wild-type GFP-Rab11-FIP2–expressing cells the claudin 2 protein was located tightly in the lateral membrane, although an increase in protein was only seen in the GFP-Rab11-FIP2WT cell line (Figure 10, B, D, and E). Claudin 4 (Figure 10, C–E) protein expression was also increased in the wild-type GFP-Rab11-FIP2– but not the GFP-Rab11-FIP2(S227E)–expressing cell line, whereas neither line exhibited a change in mRNA levels.

Of interest, whereas overexpression of the myosin Vb tail pulled in GFP-Rab11-FIP2(S227E) and Rab11a (Figure 3A), it had no affect on either E-cadherin in the adherens junction or occludin in the tight junction (Figure 11, A and B). The overexpression of GFP-Rab11a also had no effect on E-cadherin or occludin expression (Figure 11, A and B). Overexpression of the GDP-bound form of Rab11a, GFP-Rab11a(S25N), also did not affect E-cadherin (Figure 11A). These findings indicate that if a motor and Rab are involved in Rab11-FIP2's role in cellular polarity, they are not myosin Vb and Rab11a. On the basis of these results and the observation that GFP-Rab11a did not localize in the cell periphery with phospho-S227-Rab11-FIP2, we can say that the role of Rab11-FIP2 in controlling cellular polarity appears to be independent of the assembly of a myosinVb/Rab11a/Rab11-FIP2 complex.

DISCUSSION

Previous studies implicated Rab11-FIP2 in controlling the membrane trafficking of a number of cargoes through its association with Rab11a and/or myosin Vb. In this work, we elucidate a role for Rab11-FIP2 in cell polarity that does not include Rab11a or myosin Vb. Previously, we showed that Rab11-FIP2 is phosphorylated on Ser-227 by MARK2/EMK1/Par-1B (Ducharme *et al.*, 2006). Here we show that there is a decrease in phosphorylation of the serine 277 of Rab11-FIP2 in MDCK cells expressing shRNA targeted to MARK2. Mutation of Ser-227 to alanine blocked the ability of MARK2 to phosphorylate Rab11-FIP2 and retarded the establishment of cell polarity (Ducharme *et al.*, 2006). The present studies now demonstrate that the phosphorylation of Ser-227 of Rab11-FIP2 is a crucial event for both the establishment of epithelial polarity and the proper formation of cellular junctions. Previous studies demonstrated that the loss of MARK2 activity leads to deficits in the establishment of apical polarity, with the trafficking of apical membrane components to the lateral membrane, eliciting a "hepatic" phenotype (Cohen *et al.*, 2004). Similarly, in a number of cell contexts, including neuronal migration and lymphocyte migration (Mandelkow *et al.*, 2004; Lin *et al.*, 2009), deficits in MARK2 function lead to aberrant polarized cell movement. Recent studies suggested that the depolarizing effects of the *Helicobacter pylori* virulence protein CagA may accrue through its function as a pseudosubstrate inhibitor of MARK2 (Zeaiter *et al.*, 2008; Lu *et al.*, 2009; Nesic *et al.*, 2010). Although most studies focused on the possible function of MARK2 through the phosphorylation of disheveled or microtubule-associated proteins (Drewes *et al.*, 1997; Elbert *et al.*, 2006; Matenia and Mandelkow, 2009; Yamashita *et al.*, 2010; Cohen *et al.*, 2011), the present results suggest that Rab11-FIP2 is a crucial substrate for MARK2 action associated with the establishment of epithelial polarity.

In the present studies, we used antibodies specific for the MARK2 phosphorylation site on Rab11-FIP2 Ser-227 to evaluate the time course of endogenous phosphorylation during the establishment of epithelial polarity. In confluent cells, we observed phosphorylated Rab11-FIP2 in faint, dispersed puncta throughout the cells, and many times these puncta appeared in the corners of the cells. In two models of cellular polarity—wounding and calcium switch—phospho-S227-Rab11-FIP2 staining coalesced when the cells were initially reestablishing contact and dispersed as polarity was established. In the wound-healing model, phospho-S227-Rab11-FIP2 appeared in the cells at the edge of the wound near p120 plaques, similar to the lateral patch described by Nejsum and Nelson (2007). In the calcium switch model, phospho-S227-Rab11-FIP2 coalesced into internal puncta at the lateral edges between cells during the recovery from low calcium, again similar to the lateral targeting patch described by Nejsum and Nelson (2007). Of note, the phosphorylated Rab11-FIP2 dispersed after the reestablishment of polarity. These results indicate that phosphorylation of Rab11-FIP2 by MARK2 plays a specific role in the patterning of epithelial cells during the establishment of polarity.

It is also evident from the present studies that MARK2 phosphorylation likely alters the distribution or trafficking of Rab11-FIP2. GFP-Rab11-FIP2-wild type (WT) and Rab11-FIP2(S227E) in confluent MDCK cells were present on small vesicles distributed in the apical region of the cell. However, during recovery from the calcium switch, both GFP-Rab11-FIP2 chimeras located with larger and more compact puncta in both the apical and basal poles of the cell. This pattern differed from that seen with the endogenous phopho-S227-Rab11-FIP2. Although the GFP-Rab11-FIP2WT was phosphorylated on Ser-227 during recovery from calcium switch, it localized to a

more central structure within the cell, whereas faint vesicles containing the endogenous phospho-S227-Rab11-FIP2 moved laterally. The overexpressed putative pseudophosphorylated mutant, GFP-Rab1l-FIP2(S227E), also localized to a central rather than lateral structure. In these cells, unlike the GFP-Rab11-FIP2WT–expressing cells, no endogenous phospho-S227-Rab11-FIP2 was observed. We hypothesize that the pool of Rab11-FIP2 that is phosphorylated by MARK2 and involved in cell polarity is a small subset of the total Rab11-FIP2 in the cell. This subset likely interacts with a specific, rate-limiting set of proteins during cell polarization. When Rab11-FIP2 and its Ser-227 mutants are overexpressed, the balance of this interaction is altered, causing the observed changes in polarity. We are seeking to identify putative phospho-S227-Rab11-FIP2 interactors, one of which could be a phosphatase. Such a phosphatase could regulate the size of the phospho-S227-Rab11-FIP2 pool.

One known interactor with Rab11-FIP2 is the motor protein myosin Vb (Hales *et al.*, 2002). Given that Ser-227 is adjacent to the myosin Vb–binding domain of Rab11-FIP2, we investigated the possibility that phosphorylation of Ser-227 may regulate the ability of Rab11-FIP2 to bind myosin Vb. Previously, we showed that Rab11-FIP2(S227A) can still bind myosin Vb (Ducharme *et al.*, 2006), and here we showed that Rab11-FIP2(S227E) can also bind myosin Vb. Of interest, the endogenous phospho-S227-Rab11-FIP2 is not pulled into the GFP-myosin Vb tail-containing structure, and in nonpolar MDCK cells no colocalization is observed between endogenous myosin Vb and phopho-S227-Rab11-FIP2. During recovery from calcium switch endogenous phospho-S227-Rab11-FIP2 was still able to traffic to the lateral and basal areas of MDCK cells in which myosin Vb was knocked down. Thus, although our results with Rab11-FIP2(S227E) indicate that the phosphorylated form of FIP2 may be able to interact with myosin Vb, our endogenous results indicate that phospho-S227-Rab11-FIP2 is not trafficked with myosin Vb and phospho-S227-Rab11-FIP2 is spatially separated from myosin Vb.

Other known binding partners of Rab11 include the members of the Rab11 family of small GTPases. When cells overexpressing GFP-Rab11a were calcium switched, the GFP-Rab11a did not exhibit the compaction or loss of polarity that the GFP-Rab11-FIP2WT and S227E did but remained distributed in small vesicles in the apical region of the cell. In our previous work with Rab11-FIP2(S227A) (Ducharme *et al.*, 2006), the GFP-Rab11-FIP2(S227A) did not coalesce during recovery from low calcium, similar to GFP-Rab11a, but remained in vesicles throughout the cell. Work from the Stow lab implicated Rab11a in E-cadherin trafficking (Desclozeaux *et al.*, 2008). However, we did not observe any change in E-cadherin in either a GFP-Rab11a–overexpressing cell line or when MDCK cells transiently overexpressed GFP-Rab11a(S25N). Similar to our myosin Vb results, these results support the separation of Rab11-FIP2 and Rab11a during reestablishment of polarity.

Our laboratory and others have shown that alteration of proteins involved in apical trafficking and apical recycling can have profound effects on the ability of MDCK cells to form polarized epithelial cysts (Torkko *et al.*, 2008; Bryant *et al.*, 2010; Roland *et al.*, 2011). Rab11-FIP2 phosphorylated on Ser-227 can be found on vesicles within the cells of the forming and mature cysts, with concentrated densities below the apical membrane. Here we showed that mutations of Rab11-FIP2 at Ser-227 alter the formation of polarized cyst lumens in MDCK cells grown in three-dimensional culture. MDCK cells grown in Matrigel form cysts with the apical side toward the lumen, and any internal, apoptosing cells are cleared from the lumen space. Rab11-FIP2(S227A)–expressing cells were delayed in the location of the central lumen, eventually forming an outer layer of polarized cells, but were unable to clear cells from the developing lumen. In contrast, Rab11-FIP2(S227E)–expressing cells localized PCX to the adjoining membranes at the two-cell stage, but instead of forming a round lumen equally shared by all the cells, the GFP-Rab11-FIP2(S227E)–expressing cysts had an elongated, dumbbell- shaped lumen that extended between cell pairs. By the mature cyst stage, the GFP-Rab11-FIP2(S227E) cysts had formed secondary lumens within the original lumen. These results all indicate that phosphorylation of Rab11-FIP2 can alter the process of MDCK patterning and dynamic cues for lumen formation from an early stage.

To understand the implications of the changes in polarity, we examined the composition of the adherens and tight junctions. MDCK cells at steady state express both E-cadherin and K-cadherin (Stewart *et al.*, 2000). Overexpression of Rab11-FIP2(S227E), but not wild-type Rab11-FIP2 or Rab11-FIP2(S227A), caused a loss of E-cadherin, leaving K-cadherin as the main receptor of the adherens junction. We did not observe a statistically significant change in E-cadherin mRNA levels in our cell lines, nor did treatment with lysosome or proteasome inhibitors return the levels of E-cadherin to control cells. These observations may indicate another regulatory mechanism for E-cadherin expression, perhaps by microRNA-dependent regulation of translation. K-Cadherin/cadherin-6 is a member of the type II/atypical cadherin family, implicated in neural crest migration (Inoue *et al.*, 1997) and neuronal circuitry development (Inoue *et al.*, 1998; Liu *et al.*, 2008). During kidney development in both mouse and zebrafish, K-cadherin plays a role in the early aggregation of cells during mesenchyme-to-epithelial transition (Cho *et al.*, 1998; Kubota *et al.*, 2007; Liu *et al.*, 2008). Changes between E-cadherin and K-cadherin allow movement of epithelial sheets during development and organogenesis (Harris and Tepass, 2010). The results here indicate that Rab11-FIP2 phosphorylation by MARK2 not only influences the establishment of polarity, but also alters the final differentiation of epithelial cell subtypes.

The overexpression of Rab11-FIP2(S227E) also caused changes at the tight junction, with loss of occludin and a change in claudin composition. Loss of occludin without a loss of tight junction barrier or fence function is not unprecedented. Human and guinea pig Sertoli cells do not have occludin, yet form tight junctions (Moroi *et al.*, 1998). Occludin-deficient embryonic stem cells are also able to form functional tight junctions (Saitou *et al.*, 1998). Nevertheless, the alterations in claudins do suggest that phosphorylation of Rab11-FIP2 by MARK2 can regulate the composition of the cell tight junctions.

It remains unclear how expression of the phosphomimetic Rab11-FIP2(S227E) could induce the changes in the adherens and tight junctions proteins and contribute to the multilumen cyst phenotype in cells grown in three-dimensional cultures. The change to a predominance of K-cadherin within the adherens junctions of these cells could signal the cells within the main lumen to form aggregates and lumens rather than apoptosing. Of interest, occludin has been implicated in the removal of apoptosing cells from monolayers (Yu *et al.*, 2004). Thus a combination of predominantly K-cadherin–containing adherens junctions and a lack of occludin at the tight junctions could block the signal for the luminal cells to apoptose and be cleared from the lumen.

In conclusion, phosphorylation of Rab11-FIP2 on Ser-227 by MARK2 plays a critical role in the establishment of polarity in MDCK cells. Increased phosphorylation of Ser-227 in Rab11-FIP2 occurs as a transient event at the time of polarization and is diminished in stable confluent monolayers. Overexpression of the phosphomimetic Rab11-FIP2(S227E) leads to amplification of lumen formation in three-dimensional cultures and alterations in the composition of

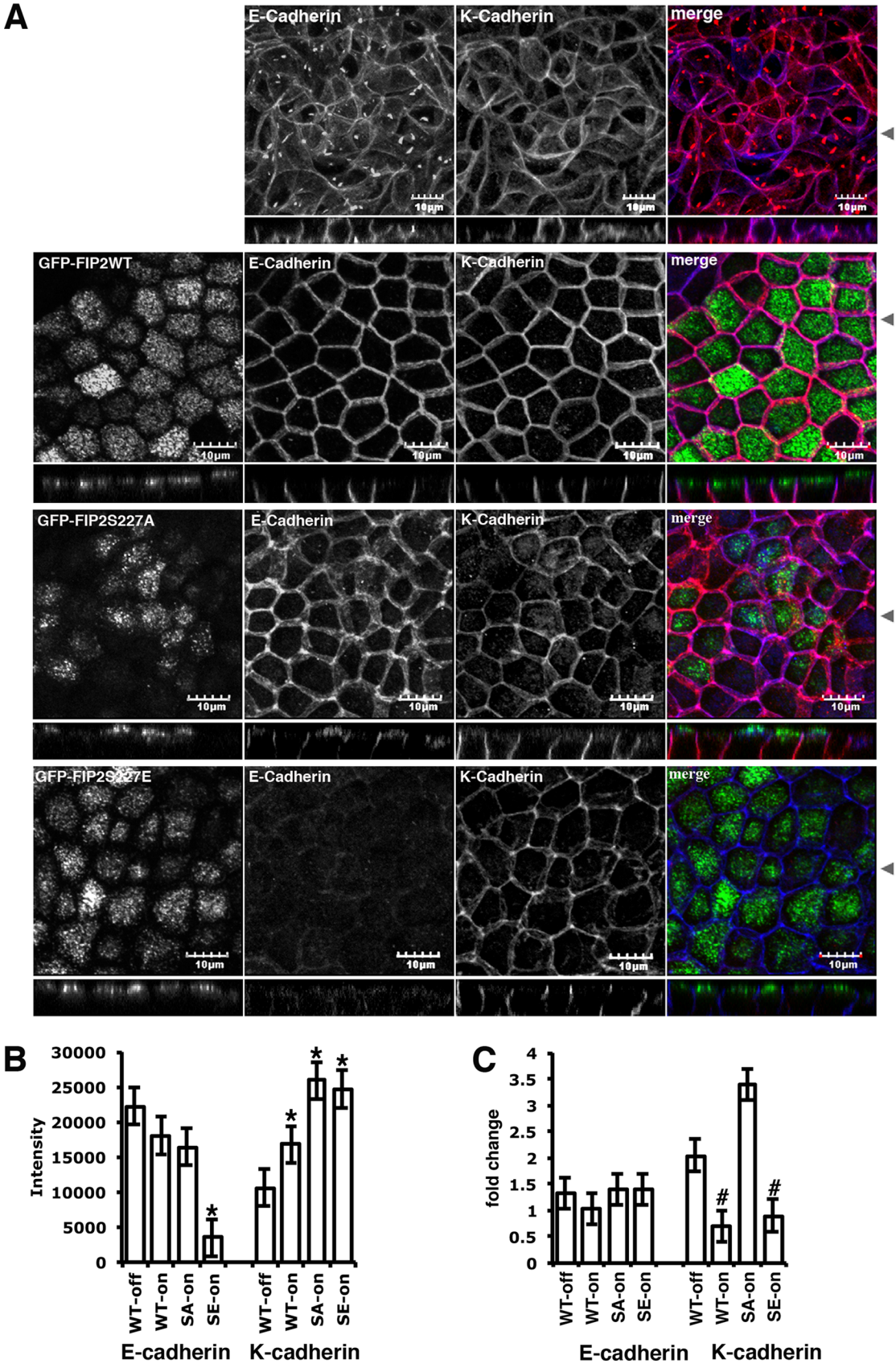

FIGURE 8: E-cadherin is lost from the adherence junction in cells overexpressing the Rab11-FIP2 phosphomimetic mutant, whereas K-cadherin remains. The GFP-FIP2 MDCK cell lines were grown on Transwell filters for 5 d postconfluence. (A) The cells were fixed and then stained for E-cadherin (red in merge) and K-cadherin (blue in merge). (B) Cells were grown as described and then lysed, run on Western blots, and probed for E-cadherin, K-cadherin, and VDAC. Three separate blots were scanned and quantified using ImageJ and normalized to control (VDAC). *p ≤ 0.009 by unpaired Student's *t* test. (C) Cells

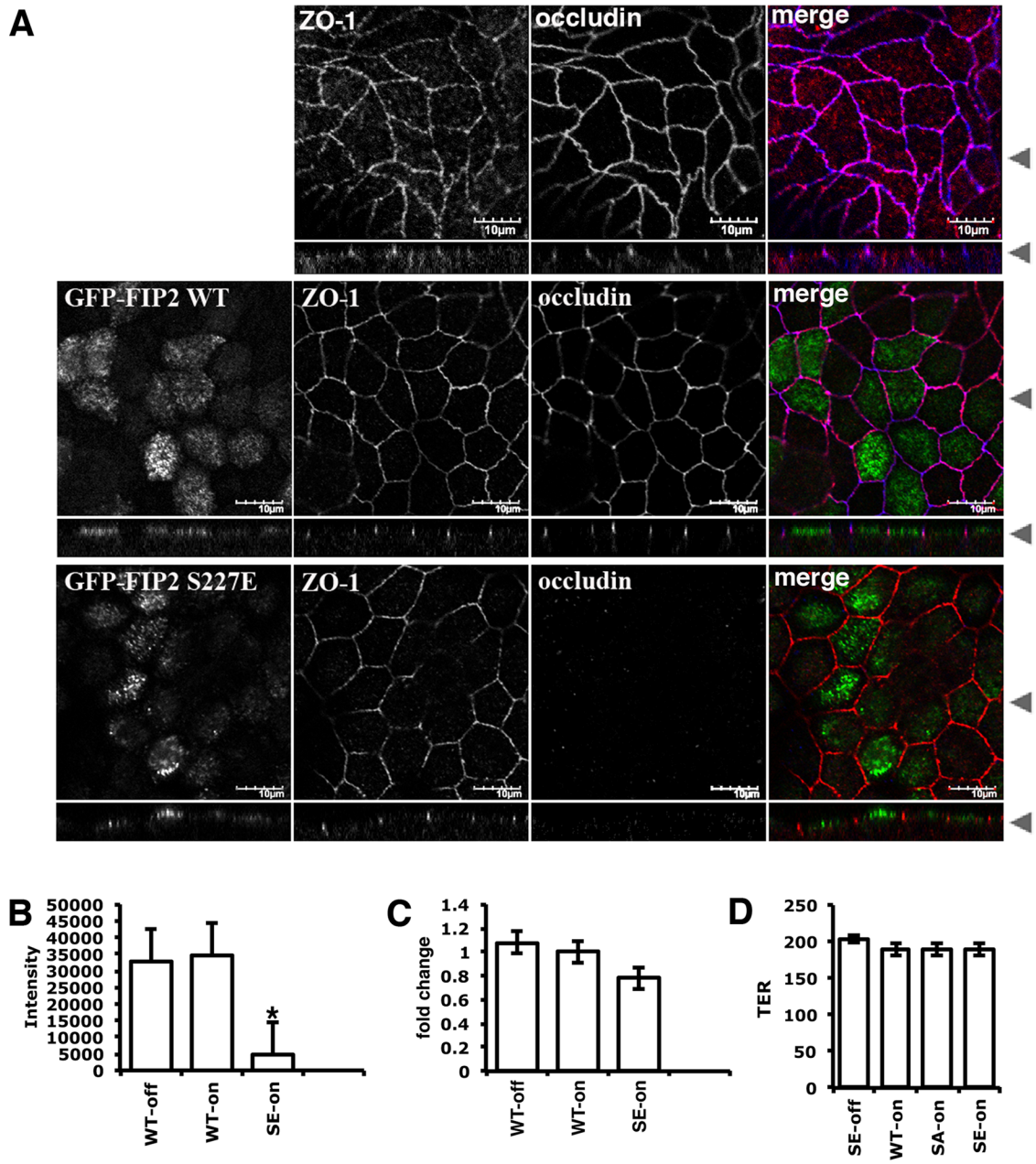

FIGURE 9: At the tight junction, Z0-1 is retained, but occludin is lost in the phosphomimetic Rab11-FIP2 (S227E) cell line. (A) Stable MDCK cell lines expressing GFP-Rab11-FIP2-WT or GFP-Rab11-FIP2 (S227E) (green in merge) were grown for 5 d postconfluence on Transwell filters, fixed, and stained for ZO-1 (red in merge) and occludin (blue in merge). (B) Cells were grown as described and then lysed, run on Western blots, and probed for occludin and VDAC. Three separate blots were scanned, quantified with ImageJ, and normalized to control (VDAC). *p = 0.0001 by unpaired Student's *t* test. (C) Cells were grown as described, and RNA was isolated and analyzed by real-time PCR. Results were normalized to GAPDH and are expressed as fold change ($2^{-\Delta\Delta CT}$). (D) TER measurements. Although all of the cell lines in the "on" condition had a drop in the TER, there were no significant differences between any of the "on" cell lines and the "off" cell lines. Arrowheads (A) indicate where the *xy* and *xz* optical slices were taken. Bar, 10 μm. Error bars indicate SEM.

adherens and tight junctions. Unlike many of the previous roles described for Rab11-FIP2 that involve Rab11a and myosin Vb, the role that Rab11-FIP2 plays in the establishment of cell polarity does not appear to involve either Rab11a or myosin Vb. The results demonstrate that Rab11-FIP2 phosphorylation is a crucial mediator of MARK2-dependent epithelial polarization.

were grown as described, and RNA was isolated and analyzed by real-time PCR. Results were normalized to glyceraldehyde-3-phosphate dehydrogenase (GAPDH) and are expressed as fold change ($2^{-\Delta\Delta CT}$). #p ≤ 0.04. Cells expressing either GFP-Rab11-FIP2-WT or GFP-Rab11-FIP2(S227A) retained both E-cadherin and K-cadherin at the junction, whereas the GFP-Rab11-FIP2(S227E)–expressing cells had mostly K-cadherin and a small amount of E-cadherin. Arrowheads indicate where the *xy* and *xz* optical slices were taken. Bar, 10 μm. Error bars indicate SEM.

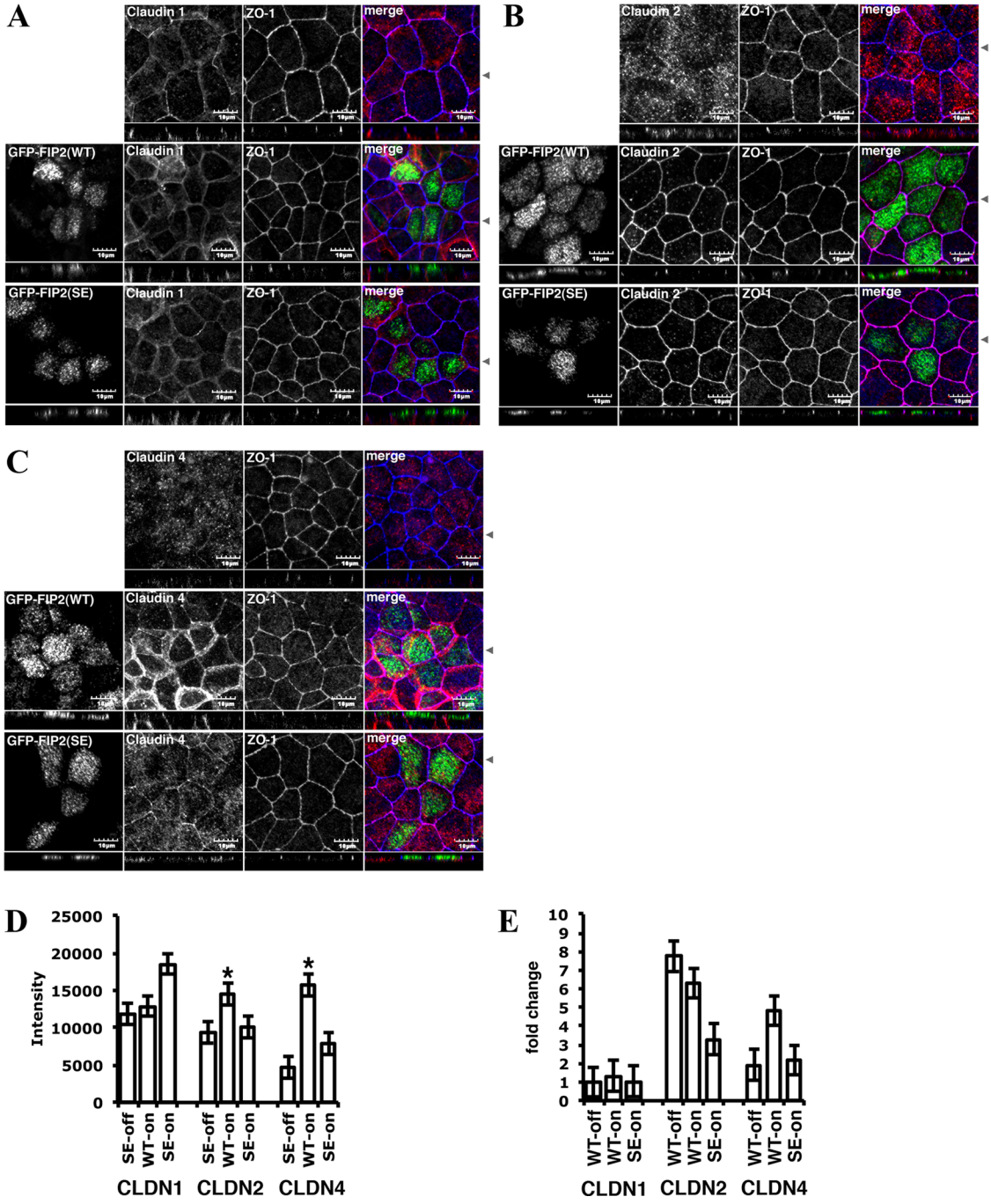

FIGURE 10: Overexpression of either GFP-Rab11-FIP2-WT or GFP-Rab11-FIP2 (S227E) altered the claudin content of tight junctions. GFP-Rab11-FIP2-WT-on and GFP-Rab11-FIP2(S227E)-on and -off were grown for 5 d postconfluence on Transwell filters. The cells were fixed then stained for claudin-1 (A), claudin-2 (B), or claudin-4 (C) and ZO-1. In the merged image, GFP-Rab11-FIP2s are pseudocolored green, the claudins are red, and ZO-1 is blue. (D) Cells were grown as described, then lysed, run on Western blots, and probed for the different claudins and VDAC. Three separate blots were scanned and quantified using ImageJ and normalized to control (VDAC). *$p \leq 0.004$ by unpaired Student's *t* test. (E) Cells were grown as described, and RNA was isolated and analyzed by real-time PCR. Results were normalized to GAPDH and are expressed as fold change ($2^{-\Delta\Delta CT}$). Bar, 10 μm. Error bars indicate SEM.

MATERIALS AND METHODS

Site-directed mutagenesis and stable line production

Site-directed mutagenesis of Rab11-FIP2 in the pEGFP vectors was performed using Pfu Turbo polymerase according to the QuikChange Site-Directed Mutagenesis Kit (Stratagene, Santa Clara, CA) with 16-min extension time. Primers were synthesized (Invitrogen, Carlsbad, CA) with one nucleotide change per oligonucleotide sequence. Previously the TCA encoding for amino acid 227 was change to GCA for the S227A mutant (Ducharme *et al.*, 2006); for the S227E mutant this GCA was mutated to GAA. Production of the doxycycline-inhibitable GFP-Rab11-FIP2(S227E) MDCK cell line was as described to Rab11-FIP2-WT and -S227A (Ducharme *et al.*, 2006). Briefly, the GFP-Rab11-FIP2(S227E) was cut out of the pEGFP vector (Clontech, Mountain View, CA) with *Nhe*I and *Sma*I and ligated into the pTRE2hyg vector (Clontech) cut with *Nhe*I and *Eco*RV. T23 MDCK cells were transfected with Effectene (Qiagen, Valencia, CA)

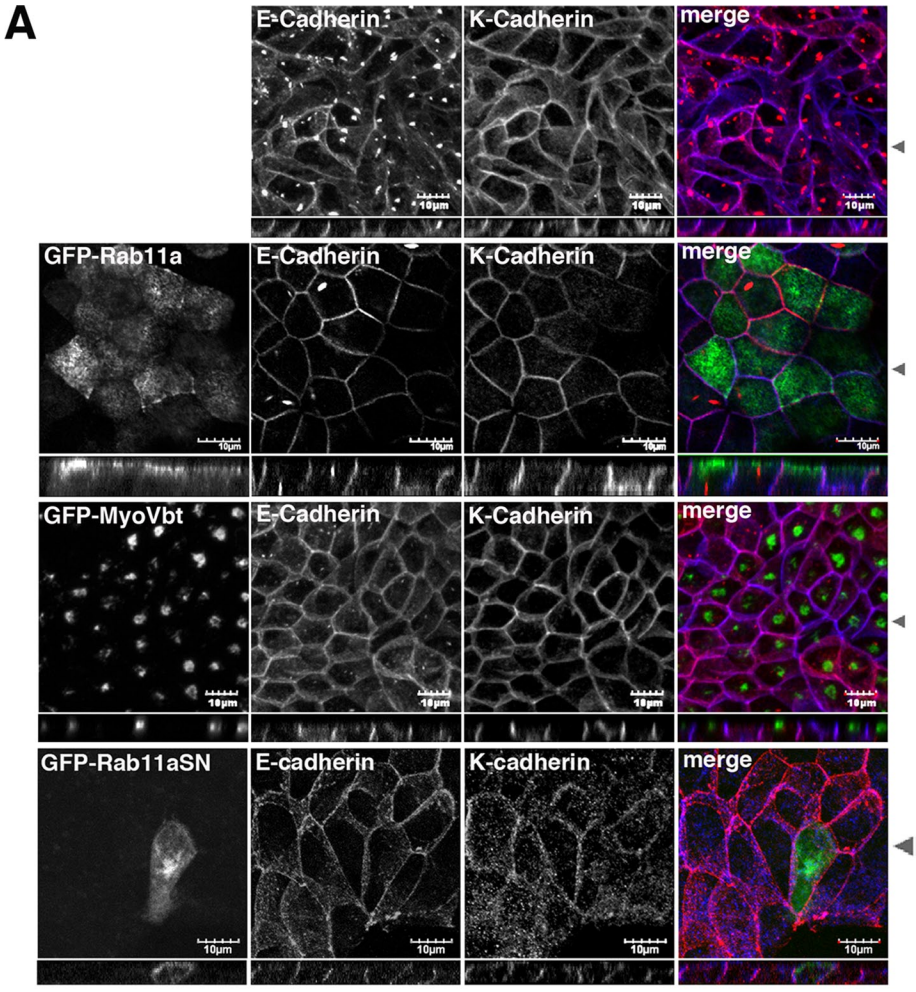

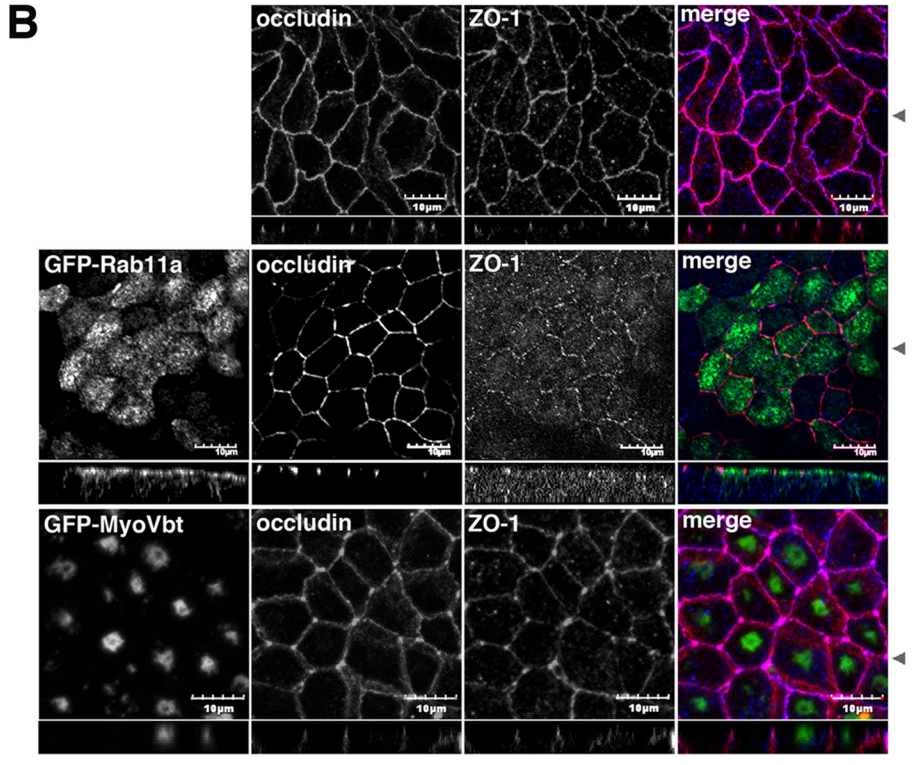

and plated in normal media. The next day the cells were trypsinized and replated in serial dilution with 0.25 ng/ml hygromycin for selection and 20 ng/ml of doxycycline for suppression of enhanced GFP (EGFP) expression. Multiple clones were selected, expanded, and initially characterized; all exhibited similar patterns and levels of EGFP-Rab11FIP2(S227E) expression. One clone was selected to use as the tetracycline-repressible stable cell line.

For this study, two lentiviral pLKO.1 shRNA vectors targeting canine MYO5B and a scrambled control shRNA were used for transduction of MDCK cells. 293T cells were plated on 10-cm dishes and grown to 30% confluence. Using Effectene, we transfected the 293T cells with the MYO5B targeting vector or scramble control, the packaging plasmid pR8.2, and the ENV plasmid pMDG.2. The 293T cells were washed in phosphate-buffered saline (PBS) after 24 h and incubated for an additional 48 h. The media from the 293T cells was then filtered and used with polybrene at 5 mg/ml to transduce plated MDCK cells at 30% confluency. The MDCK cells were then selected in media containing 2 μg/ml puromycin for 1 mo. By quantitative PCR MYO5B mRNA expression was reduced by 50% compared with the scrambled control.

Cell culture

The GFP-Rab11-FIP2 and the mutant tet-off MDCK cell lines were grown as previously described (Ducharme *et al.*, 2006) in DMEM (Cellgro, Manassas, VA) supplemented with L-glutamine (Cellgro), nonessential amino acids (Cellgro), G418 (Cellgro). and 10% fetal bovine serum (FBS; Hyclone, Logan, UT). The cell lines were also grown in the presence of 20 μg/ml doxycycline to keep them in the off position. At the time of plating for experiments the doxycycline was removed to turn on the GFP-tagged Rab11-FIP2s. The GFP-Rab11a cell line was as previously

FIGURE 11: Overexpression of GFP-Rab11a or GFP-myosin Vb tail did not disrupt E-cadherin or occludin at the apical junctions. Stable MDCK cells overexpressing either GFP-Rab11a or GFP-myosin Vb tail or transiently transfected with GFP-Rab11aS25N were grown for 5 d postconfluence on Transwell filters. The cells were fixed and then stained for either (A) E-cadherin (red in merge) and K-cadherin/cadherin-6 (blue in merge) or (B) occludin (red in merge) and ZO1 (blue in merge). Neither E-cadherin nor occludin was altered in either cell line. Bar, 10 μm.

described (Casanova *et al.*, 1999) and was grown as the GFP-Rab11-FIP2 cell lines except without doxycycline. The MARK2-KD Tet-on inducible MDCK cell line was a kind gift from Anne Musch (Elbert *et al.*, 2006). The Tet-on MARK2 MDCK cell line was grown without doxycycline to inhibit expression, and 20 μg/ml doxycycline was added to induce the shRNA expression and reduce the expression of Par-1b/MARK2. The cells were plated onto Transwells (Costar, Cambridge, MA) at confluence and then grown for 5 d before treatment. For transient expression of Cherry-myosin Vb and GFP-Rab11a(S25N), the cells were transfected (Effectene) at the time of plating onto Transwells.

For the wounding assay a pipette tip was used to remove a swath of cells down the middle of the Transwell. The cells were then washed in PBS, refed, and allowed to recover for 48 h. For the calcium switch assay the cells were washed twice in PBS and then refed in S-MEM (suspension culture; Life Technologies, Carlsbad, CA) supplemented with L-glutamine, nonessential amino acids, and 10% dialyzed FBS. The cells were then incubated for 18–24 h, refed with regular calcium media, and allowed to recover for the indicated times. For cyst growth in Matrigel (E1270; Sigma-Aldrich, St. Louis, MO), 25,000 cells were suspended in Matrigel (9.9 mg/ml stock) in either on or off media, and then 100 μl was plated into 96-well plates and allowed to grow for 1–2 wk or into Lab-Tek eight-chambered #1.0 borosilicate coverglass slides (Nunc/Thermo Fisher Scientific, Rochester, NY) and allowed to grow for 24–48 h.

Analysis of ^{125}I-IgA postendocytotic fate

The ^{125}I-IgA trafficking was as previously described (Ducharme *et al.*, 2006).

Antibodies

The rabbit anti–phospho Ser-227 Rab11-FIP2 antibody was produced and affinity purified by EZBiolab (Carmel, IN) against a phosphorylated peptide (PQRLSSAH(pS)MSDL; for validation see Supplemental Figure S1, A and B). The chicken anti–myosin Vb antibody was produced by Covance (Berkeley, CA) against a human myosin Vb–specific sequence corresponding to amino acids 943–1025 (TLSEQLSVTTSTYTMEVERLKKELVHYQQSPGEDTSLRLQEEVESLRTELQRAHSERKILEDAHSREKDELRKRVADLEQENA) and was affinity purified against the immunizing peptide (for validation see Supplemental Figure S1C). The rabbit anti–cadherin-6 (IF 1:400) was a kind gift from W. James Nelson (Stanford University School of Medicine, Stanford, CA). The mouse anti–gp135/podocalyxin (IF 1:200) was a kind gift from Karl Matlin (University of Chicago, Chicago, IL). Commercial antibodies used were as follows: from BD Transduction Laboratories (Lexington, KY), mouse anti–E-cadherin (610181, IF 1:200) and mouse anti-p120 (610133, IF 1:200); from Zymed/Invitrogen (San Francisco, CA), rabbit anti–claudin-1 (51-9000, IF 1:200), rabbit anti–claudin-2 (51-6100, IF 1:200), mouse anti–claudin-4 (32-9400, IF 1:100), rabbit anti-occludin (71-1500, IF 1:200), mouse anti-occludin (61-7300, IF 1:200), rabbit anti–ZO-1 (61-7300, IF 1:200), and mouse anti–ZO-1 (71-1500, IF 1:200); from Developmental Studies Hybridoma Bank (University of Iowa, Iowa City, IA), rat anti-ZO-1 (R26.4C, IF 1:400); and from Abcam, rabbit anti–voltage-dependent anion-selective channel protein 1 (VDAC1)/porin (Abcam, Cambridge, MA). All secondary antibodies were made in donkey and absorbed for multistaining use (Jackson ImmunoResearch Laboratories, West Grove, PA).

Transepithelial resistance measurements

Just before fixation, the TER was measured with a Millicell-ERS (Millipore, Billerica, MA) at three points within each Transwell, and then the average was used for the TER of that well.

Immunofluorescence

For claudin, ZO-1, occludin, and phosphorylated Rab11-FIP2 staining, Transwells were washed twice with PBS and then fixed with methanol for 5 min at –20°C. For myosin Vb staining the cells were fixed in 4% paraformaldehyde for 20 min at room temperature (RT). Cells were washed three times with PBS and then block-extracted for 30 min at RT in 10% normal goat serum (Jackson ImmunoResearch) and 0.3% Triton X-100 in PBS. Fixation and extraction for cadherin-6 was as previous described (Stewart *et al.*, 2000), Briefly, cells were washed three times with 0.008% SDS in PBS and then fixed in 4% paraformaldehyde for 20 min at RT. The cells were then permeabilized in CSK buffer (50 mm NaCl, 300 mm sucrose, 10 mM 1,4-piperazinediethanesulfonic acid, pH 6.8, 3 mM $MgCl_2$, 0.5% Triton X-100) for 10 min, washed three times in PBS, and then blocked in 10% normal donkey serum PBS for 30 min at RT. Transwells were incubated for either 2 h at RT or, for phosphorylated Rab11-FIP2 staining, overnight at 4°C with primary antibodies diluted in 1% normal donkey serum and 0.005% Tween-20 in PBS. Transwells were washed three times for 15 min at RT with 0.005% Tween-20 in PBS (PBS-T), then incubated for 1 h at RT with secondary antibodies diluted as described, washed three times in PBS-T and once in PBS, and then rinsed in water and mounted with ProLong Gold plus 4′,6-diamidino-2-phenylindole (DAPI; Invitrogen).

For cysts grown in Matrigel, the wells were washed three times with PBS, then fixed for 60 min at RT with 4% paraformaldehyde, and washed again with PBS. For staining, the Matrigel plugs were removed from the wells and placed in 0.5-ml microcentrifuge tubes. The plugs were block-extracted for 30 min at RT in 10% normal donkey serum rotating at RT, washed with PBS, and then incubated overnight at 4°C rotating with the primary antibodies in 1% normal donkey serum in PBS-T. The plugs were washed four times for 15 min in PBS-T at RT and incubated with secondary antibodies and Alexa-labeled phalloidin (1:100; Invitrogen) in 1% normal donkey serum in PBS-T, all rotating at RT. Plugs were washed four times in PBS-T at RT and twice in PBS at RT rotating and then mounted with ProLong gold plus DAPI between a glass slide and a coverslip. For the Lab-Tek slides all procedures were performed with the Matrigel in the chambers.

All images were captured with an Olympus FV1000 confocal microscope (Cell Imaging Shared Resource, Vanderbilt University, Nashville, TN) using a 60× oil immersion objective with an numerical aperture of 1.25 and a 3× optical zoom using the FV1000 software. The individual images were converted to tif files with the FV1000 software, and then Photoshop (Adobe, San Jose, CA) was used to produce the final figures. Mean fluorescence intensity was quantified using ImageJ (National Institutes of Health, Bethesda, MD).

Western blots

Cells were grown on Transwells for 5 d postconfluence, washed with PBS, and then lysed in CHAPS lysis buffer (1% 3-[(3-cholamidopropyl)dimethylammonio]-1-propanesulfonate, 20 mM magnesium acetate, 30 mM Tris, pH 7.5, 150 NaCl) supplemented with protease (P8340; Sigma-Aldrich) and phosphatase (P0044, P5726; Sigma-Aldrich) inhibitor cocktails for 30 min on ice. Centrifugation for 15 min at 16,000 × *g* at 4°C cleared the lysates. Protein concentration was measured with the bicinchoninic acid assay (Pierce, Rockford, IL), and 25 μg of protein was loaded onto a 10% Laemmli polyacrylamide gel (Laemmli, 1970). The proteins were transferred onto Protran Nitrocellulose Transfer Membrane (Whatman, Piscataway, NJ). Membranes were blocked for 30 min at RT with 5% dry milk powder (DMP) and 0.1% Tween-20 in Tris-buffered saline (TBS-T) and probed with primary antibodies for 2 h at RT in 2.5% DMP/TBS-T, or, for the

Oligo name	Sequence 5′ to 3′
cldn1 dog-S	GGTCAGGCTCTCTTCACTGG
cldn1 dog-AS	ATGTTGTTTTTCGGGGACAG
cldn2 dog-S	GGGCATTATTTCCTCCTTGT
cldn2 dog-AS	GGTGCTGTTCACTGGTTTTC
cldn4 dog-S	GTCCTTCTGACTGCGGAGAG
cldn4 dog-AS	AAGCGGTGAGGACAGACACT
occ dog-S	GTCCATGCTTGTCATTGTGA
occ dog-AS	AAGCCAGTTCCATAGCCTCT
E-cdh dog-S	AAAACCCACAGCCTCATGTC
E-cdh dog-AS	CACCTGGTCCTTGTTCTGGT
K-cdh dog-S	TTCCCGAAATGTCTGATGTT
K-cdh dog-AS	TACTGCTCCCTGTTTTCTCG
GAPDH dog-S	GGGAAGTCCATCTCCATCTT
GAPDH dog-AS	GAGGCATTGCTGACAATCTT

TABLE 1: Oligos used for real-time PCR.

anti–Ser-227-phosphorylated Rab11-FIP2 antibody, 1% bovine serum albumin was used instead of DMP and incubation was overnight at 4°C. Blots were washed in TBS-T, followed by a 1-h incubation with horseradish peroxidase–conjugated secondary antibodies (Jackson ImmunoResearch). Blots were washed three times in TBS-T and once in TBS, and then specific label was detected by enhanced chemiluminescence (32106; Pierce) with chemography (X-OMAT LS; Kodak, Rochester, NY). The films were scanned, and the area under the peak was calculated using ImageJ. The results were normalized to the control (VDAC), and statistical significance was determined by an unpaired Student's *t* test.

Real-time PCR analysis

RNA was isolated from the different Rab11-FIP2 MDCK cell lines using TRIzol reagent (Invitrogen) according to the manufacturer's instructions and then treated with RQ1 RNase-free DNase (Promega, Madison, WI). cDNA was synthesized using a High Capacity cDNA Reverse Transcriptase Kit (Applied Biosystems, Foster City, CA) with a mix of random and oligo dT primers. Real-time PCR was performed using a StepOnePlus real-time PCR system with Express SYBR Green ER Supermix (Applied Biosystems) and the oligo pairs listed in Table 1. All oligo pairs were from Real Time Primers (Elkins Park, PA) and validated for melting temperature and efficiency. The results were analyzed by the comparative C_T method (Schmittgen and Livak, 2008) and are expressed as $2^{-\Delta\Delta CT}$ (fold change). Statistical significance was determined by an unpaired Student's *t* test.

ACKNOWLEDGMENTS

We thank W. James Nelson for the gift of the anti–cadherin-6 antibody, Karl Matlin for the gift of the anti-gp135 antibody, and Anne Musch for the MARK2-KD cell lines. We thank Josane Sousa for her help with the qPCR analysis. Confocal fluorescence imaging was performed through scholarships for the use of the Vanderbilt University Medical Center Cell Imaging Shared Resource, supported by National Institutes of Health Grants CA68485 and DK58404. This work was supported by National Institutes of Health National Institute of Diabetes and Digestive and Kidney Diseases Grants RO1 DK048370 and RO1 DK070856 (to J.R.G.) and Grant R01 DK51970 (to G.A.).

REFERENCES

Brock SC, Goldenring JR, Crowe JE Jr (2003). Apical recycling systems regulate directional budding of respiratory syncytial virus from polarized epithelial cells. Proc Natl Acad Sci USA 100, 15143–15148.

Bryant DM, Datta A, Rodriguez-Fraticelli AE, Peranen J, Martin-Belmonte F, Mostov K (2010). A molecular network for de novo generation of the apical surface and lumen. Nat Cell Biol 112, 1035–1045.

Casanova JE, Wang X, Kumar R, Bhartur SG, Navarre J, Woodrum JE, Altschuler Y, Ray GS, Goldenring JR (1999). Association of Rab25 and Rab11a with the apical recycling system of polarized Madin-Darby canine kidney cells. Mol Biol Cell 10, 47–61.

Cho EA, Patterson LT, Brookhiser WT, Mah S, Kintner C, Dressler GR (1998). Differential expression and function of cadherin-6 during renal epithelium development. Development 12, 803–812.

Chu B-B, Ge L, Xie C, Zhao Y, Miao H-H, Wang J, Li B-L, Song B-L (2009). Requirement of myosin Vb-Rab11a-Rab11-FIP2 complex in cholesterol-regulated translocation of NPC1L1 to the cell surface. J Biol Chem 284, 22481–22490.

Cohen D, Brennwald PJ, Rodriguez-Boulan E, Musch A (2004). Mammalian Par-1 determines epithelial lumen polarity by organizing the microtubule cytoskeleton. J Cell Biol 164, 717–727.

Cohen D, Fernandez D, Lazaro-Dieguez F, Musch A (2011). The serine/threonine kinase Par1b regulates epithelial lumen polarity via IRSp53-mediated cell-ECM signaling. J Cell Biol 192, 525–540.

Cullis DN, Philip B, Baleja JD, Feig LA (2002). Rab11-FIP2, an adaptor protein connecting cellular components involved in internalization and recycling of epidermal growth factor receptors. J Biol Chem 277, 49158–49166.

Desclozeaux M, Venturato J, Wylie F, Kay JG, Joseph SR, Le HT, Stow JL (2008). Active Rab11 and functional recycling endosome are required for E-cadherin trafficking and lumen formation during epithelial morphogenesis. Am J Physiol Cell Physiol 29, 545–556.

Drewes G, Ebneth A, Preuss U, Mandelkow E-M, Mandelkow E (1997). MARK, a novel family of protein kinases that phosphorylate microtubule-associated proteins and trigger microtubule disruption. Cell 89, 297–308.

Ducharme NA, Hales CM, Lapierre LA, Ham A-JL, Oztan A, Apodaca G, Goldenring JR (2006). MARK2/EMK1/Par-1Ba phosphorylation of Rab11-family interacting protein 2 is necessary for the timely establishment of polarity in Madin-Darby canine kidney cells. Mol Biol Cell 17, 3625–3637.

Ducharme NA, Williams JA, Oztan A, Apodaca G, Lapierre LA, Goldenring JR (2007). Rab11-FIP2 regulates differentiable steps in transcytosis. Am J Physiol Cell Physiol 293, 1059–1072.

Elbert M, Cohen D, Musch A (2006). Par1b promotes cell-cell adhesion and inhibits dishevelled-mediated transformation of Madin-Darby canine kidney cells. Mol Biol Cell 17, 3345–3355.

Furuse M (2010). Introduction: claudins, tight junctions, and the paracellular barrier. In: Claudins, ed. ASL Yu, San Diego, CA: Academic Press, 1–19.

Gerardo R, Ponce A, Bolivar JJ (1991). Calcium and tight junctions. In: Tight Junctions, ed. M. Cereijido, Boca Raton, FL: CRC Press, 139–149.

Hales CM, Vaerman J-P, Goldenring JR (2002). Rab11 family interacting protein 2 associates with myosin Vb and regulates plasma membrane recycling. J Biol Chem 277, 50415–50421.

Harris TJC, Tepass U (2010). Adherens junctions: from molecules to morphogenesis. Nature 11, 502–514.

Inoue T, Chisaka O, Matsunami H, Takeichi M (1997). Cadherin-6 expression transiently delineates specific rhombomeres, other neural tube subdivisions, and neural crest subpopulations in mouse embryos. Dev Biol 183, 183–194.

Inoue T, Tanaka T, Suzuki SC, Takeichi M (1998). Cadherin-6 in the developing mouse brain: expression along restricted connection systems and synaptic localization suggest a potential role in neuronal circuitry. Dev Dyn 211, 338–351.

Jing J, Prekeris R (2009). Polarized endocytic transport: the roles of Rab11 and Rab11-FIPs in regulating cell polarity. Histol Histopathol 24, 1171–1180.

Kubota F, Murakami A, Mogi K, Yorifuji H (2007). Cadherin-6 is required for zebrafish nephrogenesis during early development. Int J Dev Biol 51, 123–129.

Laemmli UK (1970). Cleavage of structural proteins during the assembly of the head of bacteriophage T4. Nature 227, 680–685.

Lapierre LA, Kumar R, Hales CM, Navarre J, Bhartur SG, Burnette JO, Provance JDW, Mercer JA, Bahler M, Goldenring JR (2001). Myosin Vb is associated with and regulates plasma membrane recycling systems. Mol Biol Cell 12, 1843–1857.

Lin J, Hou KK, Piwnica-Worms H, Shaw AS (2009). The polarity protein Par1b/EMK/MARK2 regulates T cell receptor-induced microtubule-organizing center polarization. J Immunol 183, 1215–1221.
Lindsay AJ, McCaffrey MW (2002). Rab11-FIP2 functions in transferrin recycling and associates with endosomal membranes via its COOH-terminal domain. J Biol Chem 277, 27193–27199.
Liu Q, Londraville R, Marrs JA, Wilson AL, Mbimba T, Murakami T, Kubota F, Zheng W, Fatkins DG (2008). Cadherin-6 function in zebrafish retinal development. Dev Neurobiol 68, 1107–1122.
Lu H, Murata-Kamiya N, Saito Y, Hatakeyama M (2009). Role of partitioning-defective 1/microtubule affinity-regulating kinases in the morphogenetic activity of *Helicobacter pylori* CagA. J Biol Chem 284, 23024–23036.
Mandelkow E-M, Thies E, Trinczek B, Biernat J, Mandelkow E (2004). MARK/Par1 kinase is a regulator of microtubule-dependent transport in axons. J Cell Biol 167, 99–110.
Martin-Belmonte F, Mostov K (2008). Regulation of cell polarity during epithelial morphogenesis. Curr Opin Cell Biol 20, 227–234.
Martin-Belmonte F, Yu W, Rodriguez-Fraticelli AE, Ewald A, Werb Z, Alonso MA, Mostov K (2008). Cell-polarity dynamics controls the mechanism of lumen formation in epithelial morphogenesis. Curr Biol 18, 507–513.
Matenia D, Mandelkow E-M (2009). The tau of MARK: a polarized view of the cytoskeleton. Trends Biochem Sci 34, 332–342.
Moroi S, Saitou M, Fujimoto K, Sakakibara A, Furuse M, Yoshida O, Tsukita S (1998). Occludin is concentrated at tight junctions of mouse/rat but not human/guinea pig Sertoli cells in testes. Am J Physiol 274, C1708–C1717.
Naslavsky N, Rahajeng J, Sharma M, Jovic M, Caplan S (2006). Interactions between EHD proteins and Rab11-FIP2: a role for EHD3 in early endosomal transport. Mol Biol Cell 17, 163–177.
Nedvetsky PI *et al*. (2007). A role of myosin Vb and Rab11-FIP2 in the aquaporin-2 shuttle. Traffic 8, 110–123.
Nejsum LN, Nelson WJ (2007). A molecular mechanism directly linking E-cadherin adhesion to initiation of epithelial cell surface polarity. J Cell Biol 178, 323–335.
Nesic D, Miller MC, Quinkert ZT, Stein M, Chait BT, Stebbins CE (2010). *Helicobacter pylori* CagA inhibits PAR1-MARK family kinases by mimicking host substrates. Nat Struct Mol Biol 17, 130–132.
Roland JT, Bryant DM, Datta A, Itzen A, Mostov K, Goldenring JR (2011). Rab GTPase-Myo5B complexes control membrane recycling and epithelial polarization. Proc Natl Acad Sci USA 108, 2789–2794.
Saitou M, Fujimoto K, Doi Y, Itoh M, Fujimoto T, Furuse M, Takano H, Noda T, Tsukita S (1998). Occludin-deficient embryonic stem cells can differentiate into polarized epithelial cells bearing tight junctions. J Cell Biol 141, 397–408.
Schmittgen TD, Livak KJ (2008). Analyzing real-time PCR data by the comparative C_T method. Nat Protoc 3, 1101–1108.
Schwenk RW, Luiken JJFP, Eckel J (2007). FIP2 and Rip11 specify Rab11a-mediate cellular distribution of GLUT4 and FAT/CD36 in H9c2-hIR cells. Biochem Biophys Res Commun 363, 119–125.
Steed E, Balda MS, Matter K (2010). Dynamics and functions of tight junctions. Trends Cell Biol 20, 142–149.
Stewart DB, Barth AIM, Nelson WJ (2000). Differential regulation of endogenous cadherin expression in Madin-Darby canine kidney cells by cell-cell adhesion and activation of B-catenin signaling. J Biol Chem 275, 20707–20716.
Torkko JM, Manninen A, Schuck S, Simons K (2008). Depletion of apical transport proteins perturbs epithelial cyst formation and ciliogenesis. J Cell Sci 121, 1193–1203.
Utley TJ, Ducharme NA, Varthakavi V, Shepherd BE, Santangelo PJ, Lindquist ME, Goldenring JR, Crowe JE Jr (2008). respiratory syncytial virus uses a Vps4-independent budding mechanism controlled by Rab11-FIP2. Proc Natl Acad Sci USA 105, 10209–10214.
Yamashita K, Suzuki A, Satoh Y, Ide M, Amano Y, Masuda-Hirata M, Hayashi YK, Hamada K, Ogata K, Ohno S (2010). The 8th and 9th tandem spectrin-like repeats of utrophin cooperatively form a functional unit to interact with polarity-regulating kinase PAR-1b. Biochem Biophys Res Commun 391, 812–817.
Yu ASL, McCarthy KM, Francis SA, McCormack JM, Lai J, Rogers RA, Lynch RD, Schneeberger EE (2004). Knockdown of occludin expression leads to diverse phenotypic alterations in epithelial cells. Am J Physiol Cell Physiol 288, C1231–C1241.
Zeaiter Z, Cohen D, Musch A, Bagnoli F, Covacci A, Stein M (2008). Analysis of detergent-resistant membranes of *Helicobacter pylori* infected gastric adenocarcinoma cells revels a role for MARK2/Par1b in CagA-mediated disruption of cellular polarity. Cell Microbiol 10, 781–794.